The Behavior of Beams of Relativistic Non-Thermal Electrons Under the Influence of Collisions and Synchrotron Losses

James M. McTiernan[1]

and

Vahé Petrosian[2]

November 1989

[1]Current Address, Space Sciences Lab, University of California

[2]Department of Applied Physics, Stanford University

National Aeronautics and Space Administration Grants NSG 7092 and NGR-05-020-668

National Science Foundation Grant ATM 8320439

ABSTRACT

For many astrophysical situations, such as in solar flares or cosmic gamma-ray bursts, continuum gamma rays with energies up to hundreds of MeV have been observed, and can be interpreted to be due to bremsstrahlung radiation by relativistic electrons. The region of acceleration for these particles is not necessarily the same as the region in which the radiation is produced, and the effects of the transport of the electrons must be included in the general problem. Hence it is necessary to solve the kinetic equation for relativistic electrons, including all the interactions and loss mechanisms relevant at such energies. The resulting kinetic equation for non-thermal electrons, including the effects of Coulomb collisions and losses due to synchrotron emission, has been solved analytically in some simple limiting cases, and numerically for the general cases including constant and varying background plasma density and magnetic field. New approximate analytic solutions are presented for collision dominated cases, for small pitch angles and all energies, synchrotron dominated cases, both steady-state and time dependent, for all pitch angles and energies, and for cases when both synchrotron and collisional energy losses are important, but for relativistic electrons. These analytic solutions are compared to the full numerical results in the proper limits. These results will be useful for calculation of spectra and angular distribution of the radiation (X-rays, γ-rays and microwaves) emitted via synchrotron or bremsstrahlung processes by the electrons. We shall examine these properties and their relevance to observations in subsequent papers.

Subject headings: plasma–radiation mechanisms–Sun:flares–Sun:X-rays–X-rays:bursts

I. Introduction

In many astrophysical situations the observed electromagnetic radiation is produced by accelerated electrons with non-thermal or non-maxwellian distributions (typically with power law energy spectra and anisotropic momentum distributions). Interaction of these electrons with ambient plasma generally with varied particle, photon and magnetic field densities produces the observed radiation through synchrortron, compton or bremsstrahlung processes. In general the acceleration site, normally a region of low density, high plasma turbulence or electric field, can be different than the region where the bulk of the radiation is produced. The distribution of particles derived from modeling of the emission process is not necessarily that of the accelerated particles but is modified during the transport from one region to another. The two distributions are related by the particle kinetic equation. It is imperative then to understand the effects of transport in order to determine the distribution of the accelerated particles and to gain insight into the acceleration mechanism.

In most analyses of non-thermal sources the transport effects are either ignored or treated in an approximate manner primarily because of the complexity of the problem. Many interactions with the ambient plasma such as Coulomb collisions, inverse Compton scattering, Synchrotron cooling and interaction with both small scale electromagnetic field fluctuations (plasma waves) and large scale electric and magnetic fields can be simultaneously be important. Some simplfied cases have been analyzed. For example, in recent studies the synchrotron effects were considered by Lamb and Brainerd (1987), Coulomb collision effects by Leach and Petrosian (1981, hereafter LP) and Petrosian (1983), and synchrotron and magnetic field effects by Ho (1986) and MacKinnon and Brown (1988), In this paper we consider the effects of all three of these processes. In subsequent papers we shall apply the results from this study to microwave, X-ray and γ-ray production in solar flares, and X-ray to γ-ray production in gamma ray bursts.

We use the Fokker-Planck method for solution of the kinetic equation and determination of the distribution $f(\vec{x}, \vec{p}, t)$ in phase space. Because of the presence of

strong fields in general the particle drift across field lines is neglegible so that only the spatial coordinate s, the distance along the field line, and two components of momentum (parallel and perpendicular to the field lines) are needed. In most cases discussed below we replace the two momenta with the kinetic energy E and $\mu = \cos\alpha$ where α is the particle pitch angle. We shall also consider the steady state case which is a good approximation when the time scale of the modulation of the observed radiation is longer than the typical time scales of the transport processes. Thus we solve the kinetic equation for the distribution $f(E,\mu,s)$, where $f\,dEd\mu ds$ is the number density of particles. We utilize the Fokker-Planck treatment of the collisional effects and neglect the inverse Compton effects (which are in many ways similar to synchrotron effects), the effects of electric fields, plasma turbulence and self-absorption of synchrotron radiation.

The fully relativistic equation including collisional and synchrotron effects as well as the effects of the field inhomogeneities can then be written as

$$\mu\frac{\partial\Phi}{\partial s} - \frac{d\ln B}{2ds}\frac{\partial}{\partial\mu}[(1-\mu^2)\Phi] = \frac{1}{\beta^2}\frac{\partial}{\partial E}\left[\left(C + S\beta^3\gamma^2(1-\mu^2)\right)\Phi\right]$$
$$-\frac{S}{\beta\gamma}\frac{\partial}{\partial\mu}[\mu(1-\mu^2)\Phi] + \frac{\xi C}{\beta^4\gamma^2}\frac{\partial}{\partial\mu}\left[(1-\mu^2)\frac{\partial\Phi}{\partial\mu}\right] + \frac{\Sigma}{c\beta^2}\,, \qquad (1)$$

where $\Phi \equiv f/\beta$, $\gamma = E + 1$ is the total energy, $\beta c = c\sqrt{1-1/\gamma^2}$ is the electron velocity, B is the magnetic field strength and Σ is a source term for the injected electrons. [See, e.g., LP, Leach (1984), Petrosian (1985) and McTiernan (1989). Note that the convergence term is different here than in the equations in LP and Leach (1984), with the factor of $(1-\mu^2)$ being inside the derivative $\partial/\partial\mu$. This results in differences of less than 5% in comparison with the earlier results.]

The steps leading to equation (1) and the definition of the collisional energy loss and diffusion coefficients C and $C' = \xi C$, and the synchrotron coefficient S are given in LP and Petrosian (1985). For a background plasma of fully ionized hydrogen, $\xi = 1$ and

$$C = 4\pi r_o^2 n \ln\Lambda = 2\times 10^{-13}\left(\frac{\ln\Lambda}{20}\right)\left(\frac{n}{10^{10}\mathrm{cm}^{-3}}\right)\mathrm{cm}^{-1}\,, \qquad (2)$$

where $r_o = e^2/m_e c^2$ is the classical electron radius, n is the ambient proton or electron density, and $\ln\Lambda$ is the coulomb logarithm. This simple relation is not true for

a partially ionized plasma or a neutral gas. In these cases the ratio ξ depends on the energy; e.g., for a neutral background ξ varies from $\sim 1/12$ to $\sim 1/8$ for energies from 10 keV to 10 MeV.

The synchrotron energy loss and pitch angle change terms are proportional to

$$S = \frac{2r_o^2}{3}\left(\frac{B^2}{m_e c^2}\right) = 6.5 \times 10^{-16}\left(\frac{B}{100\ \mathrm{G}}\right)^2\ \mathrm{cm}^{-1}\ . \tag{3}$$

The coefficients S, C, and C' have the units of inverse length and are useful scales. We will find it convenient to define the ratios $R_o \equiv S/C$ ($R_o = 3230\,B^2/n$ for $\ln\Lambda = 20$), and

$$R = \beta^3\gamma^2(1-\mu^2)R_o\ . \tag{4}$$

as a measure of relative importance of the synchrotron and collisional energy losses (see Table 1).

For the source term Σ we shall assume that the electrons are injected at one point, the origin of the spatial coordinate $s = 0$, so that $\Sigma \propto \delta(s)$ is zero everywhere except at $s = 0$. Consequently we solve the equation with $\Sigma = 0$ and use the injected distribution as a boundary condition. Furthermore, we will present the results in terms of the particle flux integrated over the cross-sectional area of the loop A, given by $F = \beta c f A = \beta^2 c \Phi A$, which has units of $\mathrm{s}^{-1}\mathrm{keV}^{-1}\mathrm{ster}^{-1}$. The source, or the boundary condition at $s = 0$, is assumed to have the form

$$F(E,\mu,s=0) = F_o(E)G(\mu) = 2\alpha_o^{-2}F_o(E)e^{-(\alpha^2-\alpha_1^2)/\alpha_o^2}\ . \tag{5}$$

Here α_o^2 is the dispersion in pitch angle and α_1 is the peak direction. For lower values of α_1 and α_o the distribution becomes beamed along the field lines. For $\alpha_1 = \pi/2$ and small α_o the distribution will be of pancake form. In some cases we shall replace α^2 with $\sin^2\alpha = (1-\mu^2)$, and when necessary we shall assume a power law energy spectrum given by

$$F_o(E) = KE^{-\delta}\ . \tag{6}$$

In the next section we discuss some analytic solutions for equation (1). In Section III we describe the results from numerical solutions of this equation for a variety of

injected pitch angle distributions and field configurations. A brief summary is presented in Section IV.

II. Analytic solutions

In some limiting cases, we find that analytic solutions are possible. The analytic solutions are useful in many ways. They can give good quantitative estimates within their domain of applicability; they can be used to test the accuracy of the complex numerical results, and they provide a qualitative guide for more complicated cases outside the range of applicability.

A. Collision dominated solutions ($R \ll 1$)

For high densities and low values of the field strength and electron energy, the electron transport is dominated by Coulomb collisions and we can set $S = 0$. As shown by LP analytic solutions are then possible for small pitch angles. If $\alpha_o^2 \ll 1$, the injected electrons are strongly beamed along the field lines and we can set $\mu = (1 - \alpha^2/2)$ and $(1 - \mu^2) = \alpha^2$ in equation (1). If we ignore the $O(\alpha^2)$ terms, and define a normalized collisional column depth τ_c and energy parameter η by

$$d\tau_c = C ds \ , \qquad d\eta = \beta^2 dE \tag{7}$$

then the flux at any depth is given by equation (18) of LP:

$$F(E, \mu, \tau_c) = \left(\frac{\beta[E]}{\beta[E(\eta + \tau_c)]} \right)^2 \frac{2e^{-\alpha^2/\alpha_c^2}}{\alpha_c^2} F_o \left[E(\eta + \tau_c) \right] \ . \tag{8}$$

The pitch angle distribution is gaussian at all τ_c with a dispersion α_c given by

$$\alpha_c^2 = \alpha_o^2 + \zeta(E, \tau_c) \ , \tag{9}$$

where

$$\zeta(E, \tau_c) = 2\xi \ln \left[\frac{E(\eta + \tau_c)}{E(\eta)} \times \frac{2 + E(\eta)}{2 + E(\eta + \tau_c)} \right] \ . \tag{10}$$

From equation (7) we have $\eta = E^2/(E + 1)$ so that

$$E(x) = \frac{x}{2} \left(1 + \sqrt{1 + \frac{4}{x}} \right) \ . \tag{11}$$

Thus $E(\eta) = E$ and $[\beta(x)]^2 = 1 - 1/(x+1)^2$ relates the velocity β to energy.

1) Non-relativistic limit. For non-relativistic particles $E \ll 1$ and $\eta \approx E^2$. For $\tau_c \ll 1$, which will be the case for these particles because they lose most of their energy by $\tau_c \sim \eta \sim E^2$,

$$E(\eta + \tau_c) = E\sqrt{1 + \tau_c/E^2}$$

and

$$\zeta(E, \tau_c) = \xi \ln(1 + \tau_c/E^2) \; . \tag{12}$$

As shown by LP this solution is a good approximation up to very large values of τ_c/E^2 and for injected pitch angle distributions with values of α_o^2 up to 0.40; much larger than expected considering the assumptions made.

2) Relativistic limit. For the extreme relativistic ($E \gg 1$) electrons we have $\eta \approx E$ and $E(\eta + \tau_c) = E + \tau_c$. The diffusion in pitch angle is small and according to equations (9) and (10) the dispersion α_c^2 does not change appreciably with depth:

$$\alpha_c^2 = \alpha_o^2 + \frac{4\xi\tau_c}{E(E+\tau_c)} \; . \tag{13}$$

This implies an increase in dispersion with depth from α_o^2 to $\alpha_o^2 + 4\xi/E$ which is a small effect, except for highly beamed injection with $\alpha_o^2 E \ll 1$.

Equation (13), however, often overestimates the dispersion in pitch angle. We obtained the approximate solution equation (8) by setting $\mu = 1$ in front of the $\partial\Phi/\partial s$ term on the left hand side of equation (1). This is reasonable for the non-relativistic case where the neglected term is of order α^2 and is insignificant in comparison with the effects of the diffusion term which is of order unity. As the electron energy increases the diffusion term becomes smaller and for sufficiently high energies ($E\alpha_o^2 \gtrsim 1$) it becomes comparable to or smaller than the $O(\alpha^2)$ term neglected. Thus for relativistic electrons we need a more accurate treatment of the $\mu(\partial\Phi/\partial\tau_c)$ term. As shown in part 1 of Appendix A in this limit the diffusion term can be treated as a perturbation leading to the approximate solution ($A.4$) for extreme relativistic electrons and all angles,

$$F(E, \mu, \tau_c) = \left(\frac{\beta(E)}{\beta(E + \tau_c/\mu)}\right)^2 F_o(E + \tau_c/\mu) G(\mu) \; , \tag{14}$$

and to a more accurate solution for intermediate and high energies but for the small pitch angle regime (eq. [A.12]);

$$F(E,\mu,\tau_c) = \left(\frac{\beta[E]}{\beta[E(\eta+\tau_c)]}\right)^2 \frac{2e^{-\alpha^2/\tilde{\alpha}_c^2}}{\alpha_c^2} F_o[E(\eta+\tau_c)] \ , \tag{15}$$

where α_c^2 is given by equations (9) and (10) and the dispersion as a function of depth is

$$\tilde{\alpha}_c^2 = \frac{\alpha_c^2}{[1+\delta_e \tau_c \alpha_c^2/2(2+\eta+\tau_c)]} < \alpha_c^2 \ . \tag{16}$$

Here $\delta_e = d\ln F_o(E)/d\ln E|_{(E+\tau_c)}$ and is equal to the spectral index δ if F_o is a power law. Note that equations (15) and (16) reduce to the non-relativistic limits of equations (8) through (12) in the proper limit $\eta \sim \tau_c \ll 1$. Hence we may use this corrected solution for all energies.

Table 1 gives the values for $\tilde{\alpha}_c^2$ and α_c^2 along with α_*^2, the dispersion obtained from numerical solutions of equation (1) including only the collision terms, but without the small pitch angle approximation, for four values of α_o^2 at $\tau_c/\eta = 1$. For $\alpha_o^2 = 0.04$ the diffusion effects are more important ($4/E\alpha_o^2 \approx 5$ and $\delta\alpha_o^2/2 \approx 0.10$). Consequently, the dispersion increases with depth, while for $\alpha_o^2 = 0.40$ the reverse is true ($4/E\alpha_o^2 \approx 0.5$ and $\delta\alpha_o^2/2 \approx 1.0$) and the dispersion decreases. In all cases except for isotropic injection ($\alpha_o^2 = 40$), $\tilde{\alpha}_c^2$ provides an excellent approximation to the dispersion α_*^2. For $\alpha_o^2 \gg 1$ it is obvious that α_c^2 is not a good approximation but $\tilde{\alpha}_c^2$ provides a reasonable approximation. Figure 1 shows a comparison of the pitch angle distribution from the above analytic approximation (eqs. [15] and [16]) with that from the exact numerical solution for a power law injected flux given by equations (5) and (6) with $\delta = 5$ and $\alpha_o^2 = 0.40$. The agreement is excellent at small pitch angles, and reasonable at somewhat higher pitch angles. This comparison gives an indication of both the accuracy of our numerical code and of the usefulness of the small pitch angle approximation.

9) Flux integrated over pitch angle. In certain problems, for example those with straight magnetic field lines, and processes with isotropic cross sections, knowledge of the pitch angle distribution is not necessary. We define total flux of electrons of a given energy at a given depth to be $F_\mu(E,\tau_c) \equiv \int_{-1}^{+1} F(E,\mu,\tau_c)d\mu$ and integrate the solutions

from equation (15) to obtain

$$F_\mu(E,\tau_c) = \frac{\beta^2 F_o[E(\eta+\tau_c)]}{\beta^2[E(\eta+\tau_c)][1+\delta_e\tau_c\alpha_c^2/2(2+\eta+\tau_c)]} , \tag{17}$$

which, as shown by LP, is independent of α_o^2 for non-relativistic electrons for all values of α_o^2. For relativistic electrons, F_μ does depend on α_o^2 due to the presence of α_c^2 in the correction to the dispersion in equation (16).

The qualitative behavior of F_μ is similar for all energies. The flux is constant from $\tau_c = 0$ to $\tau_c \sim \eta$ and afterwards decreases with increasing depth. For a power law injected flux, $F_o(E) = KE^{-\delta}$, we find

$$F_\mu \approx \begin{cases} KE(E^2+\tau_c)^{-(\delta+1)/2} & \text{for } E \ll 1 \\ K(E+\tau_c)^{-\delta}/[1+\delta\tau_c\alpha_c^2/2(E+\tau_c)] & \text{for } E \gg 1 \end{cases} . \tag{18}$$

For large values of $\tau_c \gg \eta$, the flux falls off as $\tau_c^{-(\delta+1)/2}$ for $E \ll 1$ and as $\tau_c^{-\delta}$ for $E \gg 1$.

4) Spatially integrated flux. For a magnetic field which is both uniform and straight a useful quantity is $F_\tau(E,\mu)$, the flux integrated over column depth, which is defined as $F_\tau(E,\mu) \equiv \int_0^\infty F(E,\mu,\tau_c)d\tau_c$. This quantity can be sufficient for the study of spatially unresolved sources. The zeroth order approximation, equation (14), integrated over τ_c gives

$$F_\tau(E,\mu) = \mu G(\mu) \int_E^\infty (\beta')^2 F_o(E')dE' . \tag{19}$$

We cannot obtain an analytic expression for F_τ by integrating equations (8) or (15) due to the complex τ_c dependence of the dispersions α_c^2 and $\tilde{\alpha}_c^2$. It is much easier to integrate the original equation over $0 < \tau_c < \infty$. The integral of the source term Σ is equal to

$$\int_0^\infty \Sigma d\tau_c = cF_o(E,\mu) = c\beta^2\Phi_o(E,\mu) \tag{20}$$

and the equation becomes

$$\beta^2\gamma^2\frac{\partial\Phi_\tau}{\partial E} + \xi\frac{\partial}{\partial\mu}\left[(1-\mu^2)\frac{\partial\Phi_\tau}{\partial\mu}\right] - \mu\beta^4\gamma^2\Phi_o = 0 , \tag{21}$$

where $\Phi_\tau(E,\mu) \equiv \int_0^\infty \Phi(E,\mu,\tau_c)d\tau_c$.

For relativistic energies the pitch angle diffusion term is small and as above we can treat it as a perturbation. We expand Φ_τ in terms of $1/E$ and include the first order correction due to diffusion. The zeroth order solution for the flux is (since $F_\tau = c\Phi_\tau$ for $E \gg 1$)

$$F_\tau(E,\mu) = \mu \int_E^\infty F_o(E',\mu)dE' \ , \tag{22}$$

and the first order solution is

$$F_\tau(E,\mu) = \mu \int_E^\infty F_o(E',\mu)dE' + \xi \frac{\partial}{\partial \mu}\left((1-\mu^2)\frac{\partial}{\partial \mu}\left[\mu \int_E^\infty \frac{dE'}{E'^2}\int_{E'}^\infty F_o(E'',\mu)dE''\right]\right) \ , \tag{23}$$

For $F_o(E,\mu) = F_o(E)G(\mu)$ this gives

$$F_\tau(E,\mu) = \mu G(\mu)\int_E^\infty F_o(E')dE'\left(1 + \frac{\xi}{\delta_T E}\frac{1}{\mu G(\mu)}\frac{\partial}{\partial \mu}\left[(1-\mu^2)\frac{\partial}{\partial \mu}(\mu G(\mu))\right]\right) \ , \tag{24}$$

where we have defined

$$\delta_T^{-1} = \frac{E\int_E^\infty E'^{-2}dE' \int_E^\infty F_o(E'')dE''}{\int_E^\infty F_o(E')dE'} \ , \tag{25}$$

which is a measure of the energy spectral index (for a power law F_o, $\delta_T = \delta$).

For the small pitch angle regime with the injected gaussian distribution given in equation (5), we find

$$F_\tau(E,\mu) = \left[\frac{2e^{-\alpha^2/\alpha_E^2}}{\alpha_E^2(1+\alpha_o^2/2)}\right]\int_E^\infty F_o(E')dE' \ , \tag{26}$$

where

$$\alpha_E^2 = \frac{\alpha_o^2}{1+\alpha_o^2/2} + \frac{4\xi}{\delta_T E} \ . \tag{27}$$

For the power law injected energy distribution $\delta_T = \delta$ and because the dependence on energy of α_E^2 is small ($E \gg 1$), the spatially integrated flux should have a power law index equal to $\delta - 1$.

5) The total energy spectrum. Integration of F_μ over τ_c or F_τ over μ gives us the total spectrum $F_{\rm TOT}(E)$ relevant for situations with isotropic processes and spatially

unresolved observations. This solution is obtained by integrating equation (19) over $d\mu$. Thus

$$F_{\rm TOT}(E) = \int_{-1}^{+1} \mu G(\mu) d\mu \int_{E}^{\infty} (\beta')^2 F_o(E') dE' \propto \begin{cases} E^{-(\delta-2)} & \text{for } E \ll 1 \\ E^{-(\delta-1)} & \text{for } E \gg 1 \end{cases} , \qquad (28)$$

where the last relation is applicable fo a power law injected spectrum. In Section III we will compare these analytic results with numerical ones.

B. Synchrotron dominated case ($R \gg 1$)

In the opposite limit of high magnetic fields and particle energies synchrotron losses dominate. A general time dependent solution for the case with a uniform magnetic field and including synchrotron losses ($d\ln B/ds = C = 0$) is given in part 2 of Appendix A. For the steady-state case with continuous injection the result is given by equation ($A.24$). This solution is valid for electrons of all energies, but it takes a simple form for relativistic energies. The behavior of non-relativistic electrons is qualitatively similar to that of relativistic electrons.

1) Relativistic limit. The relativistic limit of equation ($A.24$) is given by equation ($A.30$), which for an injected flux of the form $F(E,\mu,0) = F_o(E)G(\mu)$ reduces to

$$F(E,\mu,s) = \frac{F_o[E/(1-\tau_s/\tau_{scr})]G(\mu)}{(1-\tau_s/\tau_{scr})^2} , \qquad (29)$$

where we have defined a dimensionless depth $\tau_s = sS$ and

$$\tau_{scr}(E,\mu) = \left(\frac{\mu}{(1-\mu^2)}\right)\frac{1}{E} . \qquad (30)$$

At a given pitch angle, $F \rightarrow 0$ at τ_{scr} which decreases with increasing energy so that higher energy particles are stripped from the beam at smaller depths. The depth s_{cr} corresponding to τ_{scr} also decreases with increasing magnetic field strength through the B^2 dependence of S.

At a given τ_s, the flux becomes zero at a critical pitch angle $\alpha_{cr} = \cos^{-1}(\mu_{cr})$ given by

$$\mu_{cr}(E,\tau_s) = \frac{1}{2\tau_s E}\left(\sqrt{1+4\tau_s^2E^2}-1\right) . \qquad (31)$$

Note that μ_{cr} increases as τ_s increases, and approaches 1 as $\tau_s \rightarrow \infty$. Electrons with higher pitch angles are stripped from the beam as the depth increases.

In order to see the initial trend of the distribution it is instructive to consider the small pitch angle regime for $\tau_s \ll \tau_{scr} = (\alpha_o^2 E)^{-1}$. In this case, we let $\mu = 1 - \alpha^2/2$ and $G(\mu) = 2\alpha_o^{-2} e^{-\alpha^2/\alpha_o^2}$ to obtain

$$F(E, \mu, s) = 2\alpha_o^{-2} F_o(E) e^{-\alpha^2/\alpha_s^2} \ , \tag{32}$$

where (unless $\delta_e < 2$)

$$\alpha_s^2 = \alpha_o^2 \left[1 + (\delta_e - 2)\alpha_o^2 \tau_s E\right]^{-1} \ , \tag{33}$$

with $\delta_e = d \ln F_o(E)/d \ln E$. The dispersion α_s^2 decreases with increasing energy, depth and magnetic field. The effects of the pitch angle term and the first order correction to the extreme relativistic approximation will add terms of order $1/E$ in the square brackets.

3) Spatially integrated flux. The general expression for the flux integrated over depth is given by equation (*A*.31). In the relativistic limit we let $\beta \rightarrow 1$ and $\beta' \rightarrow 1$ which gives

$$\begin{aligned} F_\tau(E, \mu) &= \frac{\mu G(\mu)}{(1-\mu^2)E} \int_E^\infty F_o(E') dE' \\ &= \frac{K \mu G(\mu)}{(1-\mu^2) E^{\delta+1} (\delta - 1)} \ , \end{aligned} \tag{34}$$

where the second equality is for the power law injected flux. [Note that this expression may also be obtained by integration of equation (29) over τ_s.] For a given pitch angle we have a spectral index of $(\delta + 1)$ for this case.

5) Total energy spectrum. Integration of F_τ over pitch angle (or F_μ over depth) will give the total energy spectrum. However, if $\lim_{\mu \rightarrow 1} G(\mu) \neq 0$ (e.g. isotropic injection), the resulting expression diverges. This is because electrons with zero pitch angle never lose energy or change pitch angle; thus with a continuous injection there will be an infinite number of them from $0 < s < \infty$. This divergence disappears if as $\mu \rightarrow 1$, $G(\mu) \rightarrow (1-\mu^2)^\epsilon$, $\epsilon > 0$ and the total spectrum will be the same as that in equation (34).

The divergence will also be absent in the more realistic case of finite injection time or when collisions are included.

C. Synchrotron and Collisional losses

We need to consider both synchrotron and collisional losses when the ratio of these losses [R in equation (4)] is near unity. For non-relativistic electrons $R \approx 1$ only when B is large. For relativistic electrons, however, synchrotron losses can be important for moderate values of B^2 if the density is low. There is no analytic solution for the general case including the synchrotron and collisional energy losses. Analytic solutions are possible for relativistic electrons because, as we have seen in sections A and B, Coulomb collisions and synchrotron radiation do not alter the pitch angles of relativistic electrons.

1) Relativistic limit. In this limit we can ignore the last two terms in equation (1). The solution of this equation for uniform field and constant plasma density (i.e., $E \gg 1$, $d\ln B/ds = 0$ and constant R_o) is given by equation ($A.42$) which reduces to

$$F(E,\mu,\tau_c) = F_o[E_*(E,\mu,\tau_c)]G(\mu)\frac{(1+E_*^2(E,\mu,\tau_c)/\epsilon_c^2)}{(1+E^2/\epsilon_c^2)} \ , \tag{35}$$

where

$$E_*(E,\mu,\tau_c) = E\left[\frac{1+(\epsilon_c/E)\tan(\tau_c/\mu\epsilon_c)}{1-(E/\epsilon_c)\tan(\tau_c/\mu\epsilon_c)}\right] \ , \tag{36}$$

and $\epsilon_c^{-2} \equiv R_o(1-\mu^2)$.

Note that equation (36) is valid only for $E\tan(\tau_c/\mu\epsilon_c) \leq \epsilon_c$. At a given pitch angle, $F \rightarrow 0$ at a depth given by

$$\tau'_{scr}(E,\mu) = \frac{E\tau_{scr}}{\epsilon_c}\tan^{-1}\left(\frac{\epsilon_c}{E}\right) \ , \tag{37}$$

where τ_{scr} is defined in equation (30). As in the synchrotron-dominated case, for a given energy τ'_{scr} increases as μ increases, becoming infinite at $\mu = 1$. Then particles with high pitch angles are *stripped* away and the distribution narrows as depth increases. In the limit $\epsilon_c \ll E$ (for $R_o \gg 1$) synchrotron losses dominate and the flux and the critical depth reduce to equations (29) and (30) respectively. In the opposite limit ($R_o \ll 1$,

$\varepsilon_c \gg E$) collisional losses dominate and equation (35) reduces to equation (14) as it must.

2) Spatially integrated flux. We cannot integrate the flux given in equation (36) over pitch angle due to the complex μ dependence in E_* and ε_c but it is straightforward to integrate the flux over depth. We find

$$F_s(E,\mu) = \int_0^\infty ds F(E,\mu,s) = \frac{\mu G(\mu)}{(1+E^2/\varepsilon_c^2)} \int_E^\infty F_o(E')dE'$$
$$= \frac{\mu K G(\mu)}{(1+E^2/\varepsilon_c^2)(\delta-1)E^{\delta-1}} , \qquad (38)$$

where the last relation is for the power law injected flux. In the two limits $R_o \gg 1$ and $R_o \ll 1$ this equation reduces to the expressions in equations (34) and (26) respectively.

3) Total energy spectrum. If the injected distribution is narrow (i.e., $\alpha_o^2 \ll 1$) we can integrate equation (38) over pitch angle and obtain $F_{\rm TOT}$. We find

$$F_{\rm TOT}(E) = \frac{K e^{1/R_o E^2 \alpha_o^2}}{(\delta-1)\alpha_o^2 E^{\delta+1}} \left[\ln(R_o E^2 \alpha_o^2) - 0.577 + \sum_{k=1}^{\infty} \frac{(-R_o E^2 \alpha_o^2)^{-k}}{k k!} \right] , \qquad (39)$$

which reduces to

$$F_{\rm TOT}(E) \approx \begin{cases} \dfrac{K}{(\delta-1)E^{\delta-1}} \left(1 - R_o E^2 \alpha_o^2\right) , & R_o E^2 \alpha_o^2 \ll 1 \\ \dfrac{K}{(\delta-1)R_o \alpha_o^2 E^{\delta+1}} \ln(R_o E^2 \alpha_o^2/1.78) , & R_o E^2 \alpha_o^2 \gg 1 . \end{cases} \qquad (40)$$

Thus we have the expected spectral index for the collision dominated case at low energies and the index for the synchrotron dominated case (slightly modified by due to the logarithmic term) for high energies, provided that $R_o \alpha_o^2 \sim 1$. This modification is due to the fact that collisional losses dominate for electrons with very small pitch angles, $\alpha^2 \ll 1/R_o E^2$.

D. Non-uniform field ($d\ln B/ds \neq 0$)

Next we consider a non-uniform field for which $d\ln B/ds \neq 0$. We have no solution including collisional and/or synchrotron effects and a non-uniform field. [Ho (1986) has

given numerical solutions of the equations of motion for the case including synchrotron losses and converging fields, but he has not solved the kinetic equation.] A solution for the case with $C = S = 0$ in equation (1) was given in LP for the flux per unit area of the loop. Our solution, which is integrated over the cross-sectional area of the loop is different by a factor of $B_o/B(s)$, proportional to the change of the area with depth. In the absence of other effects $B/(1-\mu^2)$ is a constant which leads to the solution

$$F(E,\mu,s) = F_o(E) G\left(\sqrt{1-(1-\mu^2)B_o/B(s)}\right) \frac{B_o}{B(s)} , \tag{41}$$

which for $G(\mu) = 2\alpha_o^{-2} e^{-(1-\mu^2)/\alpha_o^2}$, becomes

$$F(E,\mu,s) = \frac{2F_o(E)B_o}{\alpha_o^2 B(s)} \exp\left[\frac{-(1-\mu^2)B_o}{\alpha_o^2 B(s)}\right] . \tag{42}$$

At any point s, the distribution has a dispersion given by $\alpha_o^2 B(s)/B_o$; it is broadened by a factor of $B(s)/B_o$. The flux at $\alpha = 0$ is simultaneously decreased by a factor of $B_o/B(s)$, so that the number of electrons at a given depth integrated over pitch angle and area is constant with depth, as should be the case for zero energy losses. This result is independent of energy and therefore the demonstration by LP of the accuracy of the numerical code remains valid.

1) Integrated Fluxes. We can integrate the solution given in equation (42) over pitch angle to obtain

$$F_\mu(E,s) = F_o(E) . \tag{43}$$

It is clear that the energy dependence of the total flux $F_{\rm TOT}$ will be the same as that for F_o.

III. Numerical Results

We now describe results from numerical solutions of equation (1). To solve the equation we must specify the parameters of the background plasma (density and magnetic field) and the distribution of the injected electrons. We assume that electrons with the distribution given by equation (5) are injected at the top, $s = 0$, of a symmetric

magnetic flux tube and solve the equation only for $s \geq 0$. We shall use both beam ($\alpha_1 = 0$) and pancake ($\alpha_1 = \pi/2$) distributions, but we note that the latter distributions may be inherently unstable and require acceleration perpendicular to the field lines. Electrons with $\mu < 0$ at $s = 0$ are reflected back into the flux tube to simulate the symmetric geometry. Thus the total flux at $s = 0$ is equal to $F_o(E,\mu)+F(E,-\mu,0)$. The knowledge of the geometry of the flux tube is not necessary here but will be essential for the evaluation of the angular and spatial dependence of the emitted radiation.

For our purpose here all we need are the values of the coefficients $d\ln B/ds$, S and C, which can be obtained from the variation of the density and magnetic field with depth s, $B(s)$ and $n(s)$. If B and n are constant only five constants, δ, α_1, α_o^2, n_o, and $R_o = S/C$, are needed for the solution. Unless otherwise specified we assume a fully ionized hydrogen plasma with $\xi = 1$.

A. Uniform Density and Field

The parameter which determines the behavior of the electrons here is the quantity R defined in equation (4). This ratio depends on R_o and the energy and pitch angle of the electrons. We describe the effects of all these parameters by considering plasmas with different values of R_o and discuss the spectral and angular distributions at different μ and E, respectively. We shall limit our discussion to electrons with energies between 10 keV and 100 MeV.

1. Collision Dominated Models

For $R_o \ll 1$ so that $R_o\beta^3\gamma^2 \ll 1$ even for the highest energies of interest collisions dominate. Numerical results for non-relativistic electrons were given in LP and Leach (1984) and will not be reproduced here. We simply point out that the dispersion in pitch angle depends on the ratio $\tau_c/\eta \approx \tau_c/E^2$ for energies $\lesssim 300$ keV.

For higher energies such a simple scaling is no longer valid but a good approximation to the flux is given by equations (15) and (16). This is shown in Figure 2 at $\tau_c = \eta$ for a model with $R_o = 3 \times 10^{-9}$, $\delta = 5$ and $\alpha_o^2 = 0.40$ for 16 keV, 300 keV, 1 MeV and 10.6 MeV electrons. The solid lines are the numerical results for the pitch

angle distribution of the electron flux $F(\alpha)/F(\alpha = 0)$ and the o's denote the analytic results (eqs. [15] and [16]), i.e., for the same model in the limit $R_o = 0$. The pitch angle distributions broaden with increasing depth due to diffusion except for $E = 10$ MeV where diffusion is small and almost overshadowed by the higher order pitch angle term discussed in Section II.1. For all energies, the distributions are close to the analytic approximations even for angles near $\pi/2$.

In Figure 3 we show the same curves for the injected pancake distribution $\alpha_1 = \pi/2$ and $\alpha_o^2 = 0.40$. Here we have no analytic approximations. As shown by this figure, the pancake character (i.e., the maximum at $\pi/2$) is lost very quickly for low energies (at $\tau_c = \eta$). Even for the highest energy shown (10 MeV) the maximum is shifted to $\alpha \approx \pi/4$ at $\tau_c = \eta$.

i) Spatially integrated flux, F_τ. In Figure 4 we show F_τ normalized to unity at zero pitch angle for energies 300 keV and 10.6 MeV. The solid lines depict beam injection ($\alpha_1 = 0$) with $\alpha_o^2 = 0.40$, and the dashed lines $\alpha_1 = \pi/2$ and $\alpha_o^2 = 0.40$. Comparison of these curves with those in Figures 2 and 3 shows that for the beam injection, the flux at $\tau_c = \eta$ is a good representation of the total angular distribution F_τ. For the pancake injection model the maxima at both energies occur at slightly larger pitch angles for the integrated fluxes than for the flux at $\tau_c = \eta$.

ii) Pitch angle integrated flux, F_μ. In Figure 5 we plot F_μ versus normalized column depth τ_c/η for 300 keV, 1 MeV and 10.6 MeV electrons for the beam injection model with $\alpha_o^2 = 0.40$ and $\delta = 5$. The solid lines are numerical results, and the o's are the analytic results from equation (17). The agreement is good, and the behavior of F_μ is similar for all energies; for small values of τ_c/η, the flux is constant. As τ_c/η increases beyond ~ 0.2 the flux falls off, and decreases as $\tau_c^{-\delta}$ for $\tau_c/\eta \gg 1$. This behavior seems to be very general and fairly independent of the model parameters.

2. Synchrotron Dominated Models

As R increases, the synchrotron losses become more and more important and for large enough fields, they dominate even for non-relativistic electrons. As an example we eaxmine models with $R_o = 3 \times 10^3$ (or $B^2/n \approx 1$), which corresponds to $B = 10^4$G

and $n \sim 10^8 \mathrm{cm}^{-3}$, an extreme but unlikely condition for solar flares, or to $B \sim 10^{12}$G and $n \sim 10^{24}\mathrm{cm}^{-3}$, which may be representative of conditions in the magnetosphere of a neutron star. Except for very small pitch angles, synchrotron losses dominate for the entire range of energies considered here ($R \sim 1$ at 1 keV and $\alpha = \pi/4$) and the distributions behave as we expect from the solution including only synchrotron losses, i.e., equation ($A.24$), which reduces to equation (29) for $E \gg 1$. In Figure 6, we compare the numerical results (lines) with the analytic ones (o's) for 300 keV and 10.6 MeV electrons at a depth of $\tau_s = 1$ for a source distribution shown by the dashed line. The behavior of the non-relativistic electrons is qualitatively similar to that of the relativistic electrons; as the depth increases the distribution narrows and for a given depth, $F \rightarrow 0$ at some critical angle $\alpha_{cr} = \cos^{-1}(\mu_{cr})$. [See equation (31).] Note that the numerical results do not quite agree with the analytic results on the value of the critical angle. This is due to the finite size of the angular grid used for the numerical calculations; the difference between the values of the critical angle is always one grid spacing and the numerical results are inaccurate at the point next to the critical angle.

i.) Very small pitch angles: At large depths most particles acquire very small pitch angles ($\alpha \rightarrow 0$) and the numerical results begin to deviate from the analytic solution beacuse the ratio R becomes less than one and collisions become important. This effect is shown in Figure 7 in which we plot the zero pitch angle flux (actually FE^δ) versus energy for depths $\tau_s = 5$ and $\tau_s = 10$. The analytic results are shown by the dashed lines, and as we can see, for non-relativistic energies, the flux at zero pitch angle diverges as $E \rightarrow 0$. This can be deduced from equation ($A.24$) which in the zero pitch angle limit reduces to

$$F(E, \tau_s, 0) = F_o(E) G(\mu) e^{2\tau_s/\beta\gamma} \ . \tag{44}$$

The angular width of the distribution decreases exponentially;

$$\alpha_s^2 \approx 4\beta^{-2}\gamma^{-2} e^{-2\tau_s/\beta\gamma} \ , \tag{45}$$

so that the flux integrated over pitch angles, $F_\mu \propto F(\alpha = 0)\alpha_s^2$, is finite.

The analytic solution breaks down not only because the effective value of the ratio R decreases as the critical angle approaches zero, but also because the gradient of the

pitch angle distribution increases, and collisional diffusion can no longer be ignored. From equation (1) the ratio r_D, of the diffusion term to the energy loss terms (both collisional and synchrotron), is of order

$$r_D = \xi E[\beta^2\gamma^2\alpha^2(1+\beta^3\gamma^2 R_o\alpha^2)]^{-1} \ . \tag{46}$$

so that for pitch angles less than

$$\alpha_D = \left[\frac{\sqrt{4\beta E\xi R_o+1}-1}{2\beta^3\gamma^2 R_o}\right]^{1/2} \tag{47}$$

r_D exceeds unity and the analytic results are not valid. The depth at which $\alpha_D^2 = \alpha_{cr}^2$ is thus

$$\tau_{sd} = \frac{\beta\gamma}{2}\ln\frac{4}{\beta^2\gamma^2\alpha_D^2} \ . \tag{48}$$

For depths beyond τ_{sd} we do not expect the analytic solution to be useful. Table 2 gives values for α_D^2 and τ_{sd} for various energies and $R_o = 3000$.

Note that α_D^2 increases and τ_{sd} decreases with decreasing energy. For 16 keV electrons, the analytic solution is incorrect even at τ_s=1, while for 10 MeV electrons the solution may be used for large values of τ_s. This behavior is evident in Figure 7. At $\tau_s = 5$ and 10 the numerical solutions fall away from the analytic solutions for energies less than 2 MeV and 5 MeV respectively.

3. Models with Intermediate R_o

Next we consider a model with $R_o = 1.3$ ($B^2/n \sim 4\times10^{-4}$) so that synchrotron losses are important for energies greater than the rest mass energy, and collisions dominate for $E \lesssim 300$ keV. For low energies the scaling of the pitch angle distribution with τ_c/E^2 described in item 1 above is still valid. For relativistic electrons with energies $\gtrsim 5$ MeV the synchrotron energy losses dominate and we obtain distributions similar to those expected from equations (29) and (30). According to these equations, the pitch angle dispersion will be the same (or curves of F versus α will have the same shape) for depths $\tau_s \propto 1/E$. We have found that the numerical results agree with the analytic values of α_s^2 (eq. [30]) to within 10 percent for $\tau_s E = 1$.

In Figure 8 we plot the integrated flux distributions $F_\tau/F_\tau(\alpha = 0)$ for the beam (solid lines) and pancake (dashed lines) distributions with $\alpha_o^2 = 0.40$ at 300 keV and 10.6 MeV. The curves are intermediate between those given in Figures 4 and 6 with the effect of synchrotron losses evident 10.6 MeV and the effects of collisions dominant at 300 keV. Note that the pancake injection model still has a non-zero maximum, but very few electrons with $\alpha > \pi/2$.

In Figure 9 we plot $F_\mu(E, \tau)$, the flux integrated over pitch angles, versus energy for the beam and pancake distributions with $\alpha_o^2 = 0.40$ at $\tau_s = 0.1$ and 1.0. At larger depths the curves fall off at low energies due to increasing collisional losses with decreasing energy and they steepen at high energies due to increasing synchrotron losses with energy. The synchrotron losses for the pancake distribution are more noticeable because a larger proportion of the electrons have high pitch angles and therefore higher synchrotron losses.

4. Spectral index and curvature

We now discuss the spectral index of the spatially integrated flux $F_\tau(E, \mu)$. In Table 3 we give the spectral indices, slopes of power law fits of F_τ versus E curves, for different pitch angles in different energy ranges for $R_o = 3 \times 10^{-3}$ and $R_o = 1.3$. For energies $\lesssim 300$ keV, we find essentially the same angles and models with spectra for $R_o = 1.3$ in general steeper. Here collisions dominate and the slope is approximately $\delta - 1$. For relativistic energies ($E \gtrsim 10.6$ MeV), we find different behavior for the two different cases. For the beam injection and $\alpha < \pi/2$, the slope is slightly larger than $\delta - 1$ for small R, and nearly $\delta + 1$ for large R and nonzero pitch angle. These values are in good agreement with the results expected from the analytic calculations of Section 2.3. For $\alpha > 90°$, however, this slope becomes enormous, reflecting the absence of collisional diffusion for high energies. For uniform fields, very few relativistic electrons are scattered to high pitch angles.

For the pancake injection, the spectral indices are larger for relativistic energies. This is again due to the larger proportion of electrons with pitch angles near $\alpha = \pi/2$.

To show the effect of synchrotron losses, in Table 4 we give spectral indices fit to

the total integrated flux $F_{\rm TOT}(E)$ for $\delta = 5$, $\alpha_o^2 = 0.40$ for both pancake and beam injection, and for $R_o = 3 \times 10^{-9}$, 3×10^{-3}, 1.3, and 3×10^3. We see the expected results for the beam distributions; for low energies (16 to 300 keV) the index is $\sim \delta - 2$ for low fields and increases for high fields. For high energies (10 to 76 MeV) the index is $\sim \delta - 1$ for $B = 0$ and increases to slightly less than $\delta + 1$ for $B \geq 2000$ G. Thus our analytic results give accurate answers for the total flux, which is important for spatially unresolved sources.

For the pancake injection, the results are the same for the non-relativistic and semi-relativistic ranges, but as was the case for the other integrated fluxes, the spectral indices are larger for relativistic energies.

B. Uniform Density, Converging Fields

We now turn to models which have non-uniform (in particular, converging) magnetic fields. This produces two changes. First, since $d\ln B/ds$ is not zero we must include the second term in equation (1). Second, the coefficient S varies along the field lines so that R_o is no longer constant. We parametrize these models with B_o, the value of the magnetic field at $s = 0$, and the parameter $S_b = d\ln B/ds$ which we assume to be a constant; $b(s) = B(s)/B_o = \exp(sS_b)$. The effects of convergence become important when S_b is of order of the coefficients C or S for collisional and synchrotron losses, or when the dimensionless column depth $\tau_b = \int S_b ds$, which in this case is equal to $\ln b$, is greater than τ_c or τ_s. Since we have assumed constant values for S_b and C the relative importance of these two effects remains constant along the field lines but varies with the energy and pitch angle of the electrons, convergence becoming more important for higher energies and larger pitch angles. The coefficient S, however, varies along the field lines ($S = S_o b^2$) so that the relative importance of the synchrotron losses increases with depth and, of course, with energy. Thus at sufficiently large values of depth s or energy E, $\tau_s = (S_o/S_b)(b^2 - 1)/2$ exceeds τ_b and synchrotron losses become dominant.

1. Strong convergence and loss-cones

An important effect of the field convergence (when $S_b \gg C$ and S) is to produce

pitch angle distributions with distinctive "loss-cones" in the direction of the field lines. We have no analytic solution which accounts for convergence along with snychrotron radiation and collisions so we present numerical results only.

To illustrate the interplay between these processes we consider a model with isotropically injected flux (i.e., $\alpha_o^2 = \infty$), with $C = 2 \times 10^{-13}\text{cm}^{-1}$, $S_o = 6.5 \times 10^{-16}\text{cm}^{-1}$ (e.g., $B_o = 100$ G, $n_o = 10^{10}\text{cm}^{-3}$), and $S_b = 9 \times 10^{-10}\text{cm}^{-1}$, which is large enough to insure that the effects of convergence dominate over synchrotron and collisional losses for 150 keV $\lesssim E \lesssim$ 100 MeV. The pitch angle distributions at the top of the loop for 16 keV, 1 MeV and 10.6 MeV electrons are shown in Figure 10 for a model with finite length $s_{\max} = 2.4 \times 10^4$ km or $\tau_{b,\max} = 2.3$. Electrons reaching $s > s_{\max}$ are ignored. In the absence of collisional diffusion electrons with initial pitch angles $\alpha_{in} < \alpha_{cr}$ with $\sin\alpha_{cr} = b_{\max}^{-1/2}$ reach $s_{\max}$ and escape. The 10.6 MeV curve in Figure 10 shows this rapid decrease in electron flux $\alpha \lesssim 27°$ and $\alpha \gtrsim \pi - 27°$.

This effect is less pronounced at lower energies due to collisional diffusion (as shown by the 16 keV curve in Figure 10) and also for large magnetic fields and high energies due to the effectes of synchrotron losses. This is shown by the dashed line in Figure 10 for 10.6 MeV but with S increased by a factor of 40.

2. Weak convergence, relativistic electrons

In some situations the presence of convergence can have significant consequences even when convergence is not dominant. As an example we consider collision-dominated models with $C = 2 \times 10^{-6}\text{cm}^{-1}$ and $S_b = 3.7 \times 10^{-9}\text{cm}^{-1}$. In spite of the fact that $S_b \ll C$ the effect of the convergence term is approximately equal to that of the pitch angle diffusion term for relativistic electrons, and can have a significant influence in broadening the pitch angle distribution when collisions are ineffective in doing so. In Figure 11 we compare the distributions of the uniform (U) and converging (C) field models with isotropic injection, $E = 10.6$ MeV, $\tau_c = \eta$ and two values of R_o. Synchrotron losses dominate for $R_o \approx 1$ so that there are few electrons with high pitch angles and the convergence has essentially no influence. For $R_o \ll 1$, however, there are some electrons with high pitch angles at this depth and the effect of field

convergence is to increase the number of such particles even further. This effect is particularly noticeable at higher energies, but not too high an energy when synchrotron losses dominate. Even a small amount of convergence results in a substantial number of these reflected electrons as shown by the increasing divergence of the C and U curves in Figure 11 for pitch angles $\alpha > \pi/2$.

To further illustrate this effect, in Table 4 we give the values of spectral indices from power law fits to the spatially integrated flux F_r for the cases with small convergence discussed above. The values of the spectral index m_x for low energies 16 to 300 keV are similar to those of the uniform field models. At higher energies, convergence has little effect for $\alpha < \pi/2$, and the spectral indices are again similar. But for $\alpha > \pi/2$ the indices are much smaller for the converging field cases since there are more reflected electrons.

C. Solar Flare Models

It is believed that during the impulsive phase of a solar flare high energy particles (10 keV to > 10 MeV) are accelerated in a coronal magnetic loop of length 10^9 to 10^{10} cm, with density $n \approx 10^{10}$ cm^{-3} and a magnetic field of a few hundred gauss (Kundu 1983, Lu and Petrosian 1989). Below the transition region the density increases rapidly. It is not known how the magnetic field varies with depth but it is suspected to increase to a few thousand gauss at the photosphere. Above the transition region the plasma is fully ionized ($C = C'$ or $\xi = 1$) but below the transition region the temperature decreases, and the atmosphere becomes neutral.

For $n = 10^{10}$ cm^{-3} and $B_o = 100$ G, the quantity $R_o = 3 \times 10^{-3}$ at $s = 0$ and could be as large as $R_o = 0.3$ at the transition region with $\tau_c = 0.0014$ and $B_{tr} = 10^3$ G (or $\tau_b(s_{tr}) = 0.07$). Thus convergence may be important but collisional and synchrotron losses are negligible except for $E < 20$ keV and $E > 50$ MeV, respectively. Below the transition region density increases rapidly and unless the magnetic field scale height begins to decrease rapidly synchrotron and field convergence effects become negligible. In Figure 12 we plot the pitch angle distributions for 300 keV and 10.6 MeV electrons at the top of the loop (solid lines), and at $\tau_c = \eta$ (dashed lines) for models with isotropic

injection, $\delta = 5$ and $R_o = 3 \times 10^{-3}$ ($B_o = 100$ G and $n = 10^{10}\mathrm{cm}^{-3}$) at $s = 0$ which increases to $R_o = 0.3$ at the transition region. As mentioned above, the convergence will be important in the corona and at the top, we have loss-cone distributions. Below the transition region collisions dominate and we see typical behavior at both energies.

Not surprisingly, the integrated fluxes behave as in the uniform density collision dominated cases. Unless the magnetic field is very high above the transition region, there are no discernable effects of synchrotron losses on the integrated fluxes. Since $\tau_c(s_{\rm tr})/\eta \ll 1$ for most of the energy range, the integrated fluxes F_τ and $F_{\rm TOT}$ are dominated by the behavior in and below the transition region and the integrated fluxes look like those for collision dominated models.

One quantity which is readily available from observations is the energy spectral index. To show the effects of various parameters on this quantity, in Table 5 we give values for spectral indices m_γ (for energies between 10.6 and 76 MeV) and m_x (between 16 to 300 keV) of the integrated flux F_τ for models with $\delta = 5$, including: uniform field models with beam and pancake injection with $\alpha_o^2 = 0.40$ and $R_o = 3 \times 10^{-3}$ and 1.3, models with isotropic injection, $B_o = 100$ G ($R_o = 3 \times 10^{-3}$ at $s = 0$) and mirror ratios of $b_{\rm tr} = 1$, 2, 5, and 10; strongly beamed models with $\alpha_o^2 = 0.04$, $B_o = 100$ G, and $b_{\rm tr} = 2$ (to show how the effects of small convergence combine with narrow beaming); and models with $\alpha_o^2 = \infty$, $B_o = 2000$ G ($R_o(\mathrm{top}) = 1.3$), and $b_{\rm tr} = 1$ and 10. For all the weak field cases, even for low levels of convergence, and for the sharply beamed injection the values of $\Delta m = m_\gamma - m_x$ are close to zero for $\alpha > \pi/2$. For the high field case the value of Δm is larger for $\alpha > \pi/2$ and nearly as large as for the uniform weak field case. Thus we find that a high field (here $B(s_{\rm tr}) = 20{,}000$ G) can negate the effects of convergence.

Values of the spectral indices for the total integrated flux for these models are given in Table 6. For the cases with $B_o = 100$ G we find that $F_{\rm TOT}(E)$ behaves as in the collision dominated uniform field cases, since $F_{\rm TOT}$ is dominated by the behavior of the distribution below the transition region, where the collisional scale length is much smaller than the scale of convergence. For the model with $B_o = 2000$ G increased

synchrotron energy losses lead to larger slopes in all regimes.

D. Gamma-Ray Burst Models

Gamma-Ray bursts are believed to occur in the magnetospheres of neutron stars with magnetic fields ranging from 10^{12} G (as deduced from absorption lines) to less than 10^{11} G (Matz *et al.* 1985) to allow high-energy ($E >$ few MeV) γ-rays to escape without pair production. The power law energy spectra observed in some bursts to energies greater than 30 MeV are indications of the presence of non-thermal electrons accelerated to similarly high energies. These conditions require the examination of the transport of the relativistic electrons in variable magnetic fields and possibly inhomogeneous plasmas reaching densities of as high as 10^{30} electrons/cm^{-3} at the surface of the neutron stars. All three effects on the electron transport of the relativistic electrons considered here (synchrotron, collisions and field convergence) may play significant roles in this process.

If the electrons are accelerated in the magnetosphere, where R_o is expected to be very large, they suffer synchrotron losses. They quickly lose all of their perpendicular momentum and slide along the field lines with near zero pitch angles. In this phase the synchrotron loss formulae provide an accurate description of the problem up to some column depth. As shown in Section III, for large values of τ_s collisional diffusion becomes important. Since the field lines are anchored to the neutron star, the electrons hit the surface where they undergo pitch angle diffusion and emit more synchrotron or bremsstrahlung radiation if the density is very high. Equations dealing with both synchrotron and collisional processes will be applicable. It is unlikely that field convergence will play a significant role durnig this transport because the electrons will have small pitch angles and the scale height of the convergence S_b^{-1} (of the order of the neutron star radius) is probably much larger than the scales C^{-1} or S^{-1} for collisional and synchrotron process.

One can consider the problem in two steps, starting with the magnetospheric part. Consider a loop structure in the magnetosphere of a neutron star, with a magnetic field of 10^{11} G and an ambient electron density of $< 10^{24}$cm^{-3}. For this case $R_o > 32.3$, and synchrotron losses are dominant. The scale length for synchrotron processes is

$S^{-1} = 1.55 \times 10^{-3}$cm, which even for a length of about one cm gives $\tau_s > 10^3$ which is much larger that τ_{sd} (eq. [48]) where diffusion must be taken into account. [See Table 3.] We cannot calculate accurate analytic or numerical solutions for this case. The analytic solution diverges and the width becomes very small. We may, however, obtain a good approximation to F_μ, the flux integrated over pitch angle, using the analytic solution with synchrotron losses only. Collisional diffusion has no effect on the value of F_μ, therefore we expect this calculation to be useful even for extremely large values of τ_s. This flux as $\tau_s \to \infty$ can then be used as input for the second part of the problem, where we solve the full equation starting at the surface of the star.

For large τ_s the electron distribution is narrow and we may use the small angle approximation to the synchrotron-only solution. We have from equation (A.27),

$$\mathrm{X} = 1 - 2\alpha^2/\alpha_{cr}^2 \ , \tag{49}$$

where α_{cr} is given by equation (A.29). For isotropic injection, the solution equation (A.24) for the electron flux for large τ_s becomes

$$F(E, \alpha, \tau_s) = F_o(E) e^{2\tau_s/\beta\gamma} e^{-\alpha^2/\alpha_s^2} \ , \tag{50}$$

where the dispersion is given by

$$\alpha_s^2 = \frac{\alpha_{cr}^2 \beta^2 \gamma^2}{2[(\delta - 1)\gamma^2 + \delta\gamma + 3]} \ . \tag{51}$$

The width decreases and the flux for zero pitch angle increases with τ_s but the flux integrated over pitch angle is finite and is given by

$$F_\mu(E, \tau_s \to \infty) = F_o(E)[(\delta - 1)\gamma^2 + \delta\gamma + 3]^{-1} \ . \tag{52}$$

If we include collisions the flux at $\alpha = 0$ does not diverge, and the width remains finite but small. Since the width is too small to include on the pitch angle grid which we use for numerical solution, for the calculation of the flux below the surface of the star we inject all of the flux given by equation (52) at $\alpha = 0$.

The plasma at the surface is not an ordinary plasma. The electrons may be degenerate and there are heavy ions. Since the ratio ξ of the diffusion coefficient to the energy loss coefficient is highes by a factor equal to the atomic number of the ions, we have the situation in which synchrotron energy losses and collisional diffusion are important. The pitch angle distribution of 1 MeV electrons for a model with a density of Fe ions of $10^{27}\mathrm{cm}^{-3}$ and a magnetic field of 10^{12} G (or $R_o = 1.2$) is shown in Figure 13. Each curve is marked by the value of $\tau_c \approx \tau_s$ for that depth. The flux at $\tau_c = 0$ is a delta function, but the distribution is nearly isotropic even for small depths. Since this is true, when looking at any emission the important quantity is the total electron flux $F_{\mathrm{TOT}}(E)$. The spectral index at the top of the magnetospheric loop is $\delta = 3$ and the spectral indices for the delta function flux at the surface are $m_x = 2.3$, $m_m = 3.4$, and $m_\gamma = 4.7$. The indices for the total flux are $m_x = 2.6$, $m_m = 4.4$, and $m_\gamma = 5.9$. As we can see, this combination of effects (collisional diffusion plus synchrotron losses) results in steepening of the spectrum at every energy, and large breaks in the spectra between non-relativstic and relativistic energies. Such breaks have been observed in the spectra of γ-ray bursts. A detailed comparison with observations is beyond the scope of this paper and will be treated in a subsequent work.

IV. Summary

We have extended the Fokker-Planck analysis used in LP to include ultrarelativistic electrons and effects due to both collisions and synchrotron emission. We have solved the resulting kinetic equation (eq. [1]) analytically in some simple limiting cases, and have shown that the numerical results for these cases agree well with the analytic results, thus verifying the accuracy of our numerical code. We have shown that the analytic results provide a useful guide for the qualitative description of the flux distribution of the non-thermal electrons and examined the effects of non-uniformities in the magnetic field, in particular converging magnetic field geometry.

Some of the features of our results are:

(1) In situations dominated by collisions equations (15) and (16) give a fairly accurate description of energy spectra of both relativistic and non-relativistic electrons

and of the flux distribution for the gaussian pitch angle distribution of accelerated electrons. Even though these equations are small pitch angle approximations the are good for much larger angles than expected. Equations (17), (24) and (28) give the flux integrated over pitch angle, depth and both, respectively.

(2) For problems where the synchrotron process is dominant we have obtained a complete time-dependent solution (eq. [$A.21$]) and a steady state solution (eq. [$A.24$]). The relativistic limit of the latter acquires a simple form given by equations (29), (32) and (34).

(3) If both synchrotron and collisional losses are important then Equations (35), (38) and (39) give the fluxes in the relativistic limit. Analytic solutions are not possible for the less likely situation of non-relativistic energies with both synchrotron and collisional losses.

(4) The above results are for uniform magnetic fields or are applicable when the magnetic field variation scale is much larger than the scales for collisional and synchrotron losses. For cases when this is not true one must resort to numerical solutions as described in the text.

The discussion of the behavior of non-thermal electron distributions included in this paper will be important for our future work, in which we will use the numerical solutions to calculate the expected radiation during the impulsive phase for solar flares or cosmic gamma-ray bursts. Examples describing models for these bursts will be presented and we shall compare the radiation signature of such models with observations and determine the distribution of the accelerated electrons responsible for those radiations.

Acknowledgements

We would like to thank E.T. Lu and R.J. Hamilton for useful discussions and valuable insights. This work was supported by the National Aeronautics and Space Administration under grants NSG-7092 and NGR-05-020-668, and by the National Science Foundation under grant ATM 8320439.

Appendix A: Analytic Solutions

We now present some approximate analytic solutions of equation (1).

1.) Collision Dominated Solutions

Consider equation (1) with $d\ln B/ds = 0$ and $S = 0$. We have (with $d\tau_c = Cds$)

$$\mu\frac{\partial\Phi}{\partial\tau_c} - \frac{\partial\Phi}{\partial E} = \frac{\xi}{E^2}\frac{\partial}{\partial\mu}\left[(1-\mu^2)\frac{\partial\Phi}{\partial\mu}\right] , \qquad (A.1)$$

where $\xi = C'/C(= 1$ for a fully ionized background plasma). The small pitch angle solution for non-relativistic electrons is given in the text. This solution (eq. [8]) cannot be extended to high energies because as E increases the term ignored (of order $\alpha^2\partial\Phi\partial s$) becomes more important relative to the diffusion term. For extreme relativistic electrons we may ignore the pitch angle diffusion term on the right hand side of equation $(A.1)$, and we have

$$\mu\frac{\partial\Phi}{\partial\tau_c} - \frac{\partial\Phi}{\partial E} = 0 , \qquad (A.2)$$

which for injected $\Phi(E,\mu,0) = \Phi_o(E)G(\mu)$ has the solution

$$\Phi(E,\mu,\tau_c) = \Phi_o(E+\tau_c/\mu)G(\mu) . \qquad (A.3)$$

For relativistic energies, $\beta = 1$ and $F = c\Phi$. In the small pitch angle regime and for a gaussian pitch angle distribution $G(\mu) = 2\alpha_o^{-2}e^{\alpha^2/\alpha_o^2}$, equation $(A.3)$ gives

$$F(E,\mu,\tau_c) = F_o(E+\tau_c)\frac{2e^{-\alpha^2/\alpha_o^2}}{\alpha_o^2}\left[1+\frac{\delta_e\tau_c\alpha^2}{2(E+\tau_c)}\right]^{-1} , \qquad (A.4)$$

where $\delta_e = d\ln F_o(E)/d\ln E|_{E+\tau_c}$ and is equal to the spectral index when F_o is a power law. Note that the term in the brackets which is of order $\delta_e\alpha_o^2$ has an effect which is opposite of the diffusion term; namely that dispersion decreases with increasing depth τ_c.

For lower energies or smaller α_o^2 the diffusion term becomes important and in the intermediate energies it increases the dispersion with depth at a rate determined by the value of $1/E\alpha_o^2$. To account for this effect we treat the pitch angle diffusion term as a

perturbation. The fractional perturbation we denote by ϕ_1. In the small pitch angle regime ϕ_1 obeys the equation

$$\frac{\partial \phi_1}{\partial \tau_c} - \frac{\partial \phi_1}{\partial E} = \frac{4\xi}{E^2 \alpha_x^2} \left(\frac{\alpha^2 - \alpha_x^2}{\alpha_x^2} \right) , \tag{A.5}$$

where

$$\alpha_x^2 = \frac{\alpha_o^2}{1 + \delta \alpha_o^2 / 2(E + \tau_c)} ; \tag{A.6}$$

the solution of this is

$$\phi_1 = \frac{4\xi}{\alpha_o^2} \left(\frac{\alpha^2 - \alpha_x^2}{\alpha_x^2} \right) \frac{\tau_c}{E(E + \tau_c)} . \tag{A.7}$$

Combining this with equation (A.4) we then obtain, in the small pitch angle regime,

$$F(E, \mu, \tau_c) = F_o(E + \tau_c) \frac{2e^{-\alpha^2/\tilde{\alpha}_c^2}}{\alpha_c^2} , \tag{A.8}$$

where

$$\alpha_c^2 = \alpha_o^2 + [4\xi \tau_c / E(E + \tau_c)] , \tag{A.9}$$

and

$$\tilde{\alpha}_c^2 = \frac{\alpha_c^2}{[1 + \delta_e \tau_c \alpha_c^2 / 2(E + \tau_c)]} . \tag{A.10}$$

This form is similar to the non-relativistic solution (equations [8] through [10] in the text). With a small modification of $\tilde{\alpha}_c^2$ to the form

$$\tilde{\alpha}_c^2 = \frac{\alpha_c^2}{[1 + \delta_e \tau_c \alpha_c^2 / 2(2 + \eta + \tau_c)]} , \tag{A.11}$$

with α_c^2 given by equations (9) and (10), and addition of the velocity factors as in equation (8) we can combine the solutions of the two limiting cases as

$$\begin{aligned} F(E, \mu, \tau_c) &= \left(\frac{\beta[E]}{\beta[E(\eta + \tau_c)]} \right)^2 \frac{2e^{-\alpha^2/\alpha_c^2}}{\alpha_c^2} F_o[E(\eta + \tau_c)][1 + \delta_e \tau_c \alpha^2 / 2(2 + \eta + \tau_c)] \\ &= \left(\frac{\beta[E]}{\beta[E(\eta + \tau_c)]} \right)^2 \frac{2e^{-\alpha^2/\tilde{\alpha}_c^2}}{\alpha_c^2} F_o[E(\eta + \tau_c)] , \end{aligned} \tag{A.12}$$

which describes the solution with a high degree of accuracy and to much larger values of the pitch angle than expected considering the small pitch angle approximation.

2.) The Uniform Field Synchrotron Solution

It is well known (see e.g., Jackson 1962) that the rate of change in $\beta_\parallel \equiv \beta\mu$, the velocity parallel to the magnetic field, due to synchrotron losses is zero; i.e., $(\dot{\beta}_\parallel)_s = 0$. If collisional losses are neglegible and the B field is uniform, it is then convenient to rewrite the kinetic equation in terms of $\beta_\parallel$ and $\beta_\perp \equiv \beta(1-\mu^2)^{1/2}$. Furthermore, since $\beta_\parallel$ is constant the time dependence can easily be incorporated and equation $(A.1)$ becomes

$$\left(\frac{\partial}{\partial ct} + \beta_\parallel \frac{\partial}{\partial s}\right) \tilde{f} = \frac{\partial}{\partial \beta_\perp}\left[S\beta_\perp(1-\beta_\perp^2-\beta_\parallel^2)^{1/2}\tilde{f}\right] \ . \qquad (A.13)$$

The function $\tilde{f}$ is now the distribution function in terms of $(\beta_\parallel, \beta_\perp)$ and we can use the Jacobian of the transformaton from (E,μ) to $(\beta_\parallel, \beta_\perp)$ to give us the relation between $\tilde{f}$ and f, the distribution in terms of (E,μ);

$$\tilde{f}(\beta_\parallel, \beta_\perp) = \left[\tilde{\gamma}^3(1-\tilde{\mu}^2)^{1/2} f(\tilde{E}, \tilde{\mu})\right] \ , \qquad (A.14)$$

The tilde denotes quantities which are to be functions of $(\beta_\parallel, \beta_\perp)$; i.e., $\tilde{\gamma} = (1-\beta_\parallel^2 - \beta_\perp^2)^{-1/2}$, $\tilde{E} = \tilde{\gamma} - 1$, and $\tilde{\mu} = \beta_\parallel/(\beta_\parallel^2+\beta_\perp^2)^{1/2}$. If we make the substitution

$$\tilde{h} = \beta_\perp(1-\beta_\perp^2-\beta_\parallel^2)^{1/2}\tilde{f} = \tilde{\gamma}(\tilde{\gamma}^2-1)^{1/2}(1-\tilde{\mu}^2) f(\tilde{E},\tilde{\mu}) \ , \qquad (A.15)$$

and define $y = ctS$ and $\tau_s = sS$ equation $(A.13)$ becomes

$$\frac{\partial \tilde{h}}{\partial y} + \beta_\parallel \frac{\partial \tilde{h}}{\partial \tau_s} = \beta_\perp(1-\beta_\perp^2-\beta_\parallel^2)^{1/2}\frac{\partial \tilde{h}}{\partial \beta_\perp} \ . \qquad (A.16)$$

We define a new variable u by

$$du = \frac{d\beta_\perp}{\beta_\perp(1-\beta_\perp^2-\beta_\parallel^2)^{1/2}} \ , \qquad (A.17)$$

so that

$$u = -\gamma_\parallel \mathrm{sech}^{-1}(\gamma_\parallel \beta_\perp) \quad \text{and} \quad \beta_\perp = \frac{1}{\gamma_\parallel}\mathrm{sech}\left(-u/\gamma_\parallel\right) \ , \qquad (A.18)$$

where $\gamma_\parallel \equiv (1-\beta_\parallel^2)^{-1/2}$. Equation $(A.13)$ is simplified to

$$\frac{\partial \tilde{h}}{\partial y} + \beta_\parallel \frac{\partial \tilde{h}}{\partial \tau_s} = \frac{\partial \tilde{h}}{\partial u} \ . \qquad (A.19)$$

If at $\tau_s = 0$ the distribution is given by $g(y)f_o(E,\mu)$ so that

$$\tilde{h}_o(u,0,y) = \left[\tilde{\gamma}(\tilde{\gamma}^2-1)^{1/2}(1-\tilde{\mu}^2)f_o(\tilde{E},\tilde{\mu})\right]_{\tilde{E}(u),\tilde{\mu}(u)} , \qquad (A.20)$$

Equation $(A.13)$ has the simple solution $\tilde{h}(u,\tau_s,y) = g(y-\tau_s/\beta_\parallel)\tilde{h}_o(u+\tau_s/\beta_\parallel)$, and the distribution function in terms of energy and pitch angle $f = \tilde{h}(u,\tau_s,y)/\beta\gamma^2(1-\mu^2)$ is

$$f(E,\mu,\tau_s,y) = \frac{g(y-\tau_s/\beta_\parallel)}{\beta\gamma^2(1-\mu^2)}\left[\tilde{\gamma}(\tilde{\gamma}^2-1)^{1/2}(1-\tilde{\mu}^2)f_o(\tilde{E},\tilde{\mu})\right]_{\tilde{E}(u+\tau_s/\beta_\parallel),\tilde{\mu}(u+\tau_s/\beta_\parallel)} . \qquad (A.21)$$

It is easy to show that

$$\tilde{E}(u+\tau_s/\beta_\parallel) = \tilde{E}(\mathrm{X}) = (\gamma_\parallel - \mathrm{X})/\mathrm{X}$$

and

$$\tilde{\mu}(u+\tau_s/\beta_\parallel) = \tilde{\mu}(\mathrm{X}) = \beta_\parallel\gamma_\parallel/(\gamma_\parallel^2-\mathrm{X}^2)^{1/2} , \qquad (A.22)$$

where

$$\mathrm{X}(E,\mu,\tau_s) = \tanh\left(\frac{|u|-\tau_s/\beta_\parallel}{\gamma_\parallel}\right) = \frac{\gamma_\parallel - \gamma\tanh(\tau_s/\beta_\parallel\gamma_\parallel)}{\gamma-\gamma_\parallel\tanh(\tau_s/\beta_\parallel\gamma_\parallel)} . \qquad (A.23)$$

Returning to the time independent case of continuous injection, for which $g(y)$ is a constant, we find for the flux $F = \beta cf$

$$F(E,\mu,\tau_s) = \frac{\gamma_\parallel^2 F(\tilde{E}(\mathrm{X}),\tilde{\mu}(\mathrm{X}),0)}{\gamma^2(1-\mu^2)}\left(\frac{1-\mathrm{X}^2}{\mathrm{X}^2(\gamma_\parallel^2-\mathrm{X}^2)}\right) , \qquad (A.24)$$

where $F(E,\mu,0)$ is the injected flux.

At $\tau_s = 0$, $\mathrm{X} = \gamma_\parallel/\gamma$, with increasing τ_s, X and the flux F decrease monotonically and become zero at a depth given by

$$\tau_{scr} = \frac{\beta_\parallel\gamma_\parallel}{2}\ln\left(\frac{\gamma+\gamma_\parallel}{\gamma-\gamma_\parallel}\right) . \qquad (A.25)$$

The value of τ_{scr} decreases with increasing energy; particles with higher energy travel shorter distances, and for a given energy τ_{scr} is smallest at $\mu = 0$; particles with high pitch angles lose energy more quickly than those with smaller pitch angles.

At a given depth τ_s, the flux approaches zero at a critical value of the pitch angle $\alpha_{cr} = \cos^{-1}(\mu_{cr})$ which we may calulate by solving the trancendental equation

$$\tanh^{-1}\left[\frac{1}{\gamma(1-\beta^2\mu_{cr}^2)^{1/2}}\right] = \frac{\tau_s(1-\beta^2\mu_{cr}^2)^{1/2}}{\beta\mu_{cr}} \ . \qquad (A.26)$$

For large depths $\tau_s \to \infty$, $\mu_{cr} \to 1$, and the distribution becomes infinitely narrow, and at the same time,the flux at $\mu = 1$ gets infinitely large. For $\mu \to 1$, or $\alpha^2 \to 0$, we have

$$\mathrm{X} = 1 - \frac{\beta^2\gamma^2\alpha^2 e^{2\tau_s/\beta\gamma}}{2} \ , \qquad (A.27)$$

$\tilde{E}(\mathrm{X}) = E$, $\tilde{\mu}(\mathrm{X}) = \mu$, and

$$F(E, \mu = 1, \tau_s) = F(E, 1, 0)e^{2\tau_s/\beta\gamma} \ . \qquad (A.28)$$

For $\alpha_{cr} \ll 1$, we may solve equation $(A.26)$ and find value for the critical angle given by

$$\alpha_{cr}^2 = \frac{4e^{2\tau_s/\beta\gamma}}{\beta^2\gamma^2} \ . \qquad (A.29)$$

Even though the flux at $\alpha = 0$ diverges for large depths, the width becomes zero, so that the flux integrated over pitch angle, which is of order $F(\mu = 1)\alpha_{cr}^2$, remains finite.

The solution has a particularly simple form for ultrarelativistic electrons. We let $\beta \to 1$ in equation $(A.21)$ and find $\mathrm{X} = \gamma_{\parallel}(1 - \tau_s/\tau_{scr})/\gamma \ll 1$, $\mu(\mathrm{X}) = \mu$, and if $F(E, \mu, 0) = F_o(E)G(\mu)$ then

$$F(E, \mu, s) = \frac{F_o[E/(1-\tau_s/\tau_{scr})]G(\mu)}{(1-\tau_s/\tau_{scr})^2} \ , \qquad (A.30)$$

where $\tau_{scr} = \mu/E(1-\mu^2)$. This solution is discussed in Section II.

In Section II we discuss the flux integrated over depth for given pitch angles. This would pertain to the case for which the field lines are straight and for spatially unresolved observations. We may obtain the flux integrated over depth either by integration of the solution in equation $(A.30)$ over τ_s or by solution of the full equation (eq. [A.13]) integrated over τ_s. We find

$$F_\tau(E, \mu) \equiv \int_0^\infty F(E, \mu, \tau_s)d\tau_s = \frac{\beta\mu}{\gamma^2(1-\mu^2)}\int_E^\infty dE' \frac{F_o(E')}{\beta'^2} G\left(\frac{\beta\mu}{\beta'}\right) \ , \qquad (A.31)$$

where we must keep $\beta_\parallel$ constant in the integrand. The integration is complex for the general case due to the complex dependence on β' in the integrand. For an initially isotropic distribution, $G(\beta\mu/\beta')$ is constant and $F_s \propto \int_E^\infty \beta'^{-2} F_o(E')dE'$.

3.) The Relativistic Energy Loss Solution

As in the collisional case, the synchrotron pitch angle change term is much less than the energy loss term for $E \gg 1$. The relativistic electrons lose energy at constant pitch angle until they become non-relativistic when the collisional diffusion and $\dot{\mu}_s$ terms become important. Here we ignore these terms, keeping in mind that we can add those terms as perturbations as in item (1.) above if neccesary. We take the limit $\beta \to 1$ and let $d\ln B/ds = 0$ in equation (1). If we define $\varepsilon_c^2 \equiv C/S(1-\mu^2)$, then

$$\mu\frac{\partial\Phi}{\partial\tau_c} = (1 + E^2/\varepsilon_c^2)\frac{\partial\Phi}{\partial E} + 2\varepsilon_c^{-2}E\Phi \ , \tag{A.32}$$

and if $d\eta \equiv dE/(1 + E^2/\varepsilon_c^2)$, then

$$\eta = \varepsilon_c \tan^{-1}(E/\varepsilon_c) \ , \quad E(\eta) = \varepsilon_c \tan(\eta/\varepsilon_c) \ , \tag{A.33}$$

and

$$\mu\frac{\partial\Phi}{\partial\tau_c} = \frac{\partial\Phi}{\partial\eta} + \frac{2}{\varepsilon_c}\tan\left(\frac{\eta}{\varepsilon_c}\right)\Phi \ . \tag{A.34}$$

Next we let $\Phi(\eta,\mu,\tau_c) = \phi(\rho)\psi(\eta)$ where $\rho \equiv \eta + \tau_c/\mu$ so that

$$\mu\left.\frac{\partial\Phi}{\partial\tau_c}\right|_\eta = \psi\frac{d\phi}{d\rho} \ , \quad \left.\frac{\partial\Phi}{\partial\eta}\right|_{\tau_c} = \psi\frac{d\phi}{d\rho} + \phi\frac{d\psi}{d\eta} \ , \tag{A.35}$$

and equation (A.34) reduces to

$$\frac{d\psi}{d\eta} = -\frac{2}{\varepsilon_c}\tan\left(\frac{\eta}{\varepsilon_c}\right)\psi \tag{A.36}$$

which has the solution

$$\psi(\eta) = \psi_o \sec^{-2}(\eta/\varepsilon_c) \ . \tag{A.37}$$

This gives

$$\Phi(\eta,\mu,\tau_c) = \phi(\rho)\psi_o \sec^{-2}(\eta/\varepsilon_c) \ , \tag{A.38}$$

where ψ_o is a constant of integration.

For the initial condition

$$\Phi(E,\mu,0) = \phi(\rho=\eta)\psi(\eta) = c^{-1}F_o[E(\eta)]G(\mu) \tag{A.39}$$

we then find

$$\phi(\eta)\psi_o = c^{-1}G(\mu)F_o[\varepsilon_c\tan(\eta/\varepsilon_c)]\sec^2(\eta/\varepsilon_c)\ . \tag{A.40}$$

Thus

$$\phi(\rho) = \frac{F_o[\varepsilon_c\tan(\rho/\varepsilon_c)]G(\mu)\sec^2(\rho/\varepsilon_c)}{c\psi_o} \tag{A.41}$$

and, finally

$$F(E,\mu,\tau_c) = c\Phi(E,\mu,\tau_c) = \frac{c\phi(\rho)\psi_o}{\sec^2(\eta/\varepsilon_c)} = \frac{F_o[\varepsilon_c\tan(\rho/\varepsilon_c)]G(\mu)\sec^2(\rho/\varepsilon_c)}{\sec^2(\eta/\varepsilon_c)}\ . \tag{A.42}$$

We substitute for ρ and η to obtain the flux int terms of E and μ;

$$F(E,\mu,\tau_c) = F_o[E_*(E,\mu,\tau_c)]G(\mu)\frac{(1+E_*^2(E,\mu,\tau_c)/\varepsilon_c^2)}{(1+E^2/\varepsilon_c^2)}\ , \tag{A.43}$$

where

$$E_*(E,\mu,\tau_c) = \varepsilon_c\left[\frac{E+\varepsilon_c\tan(\tau_c/\mu\varepsilon_c)}{\varepsilon_c - E\tan(\tau_c/\mu\varepsilon_c)}\right]\ . \tag{A.44}$$

References

Brown, J.C. and Melrose, D.B. 1977, *Solar Phys.*, **73**, 117.

Chupp, E.L., Forrest, J.M., Ryan, M.L., Cherry, C., Reppin, C., Kanbach, G., Riger, E., Pinkau, K., Share, G.H., Kinzer, R.L., Strickman, M.S., Johnson, W.N. and Kurfess, J.D. 1981, *Ap. J. (Letters)*, **244**, L171.

Dermer C.D. and Ramaty R. 1986, *Ap. J.*, **301**, 962.

Dermer, C.D. 1987, *Ap. J.*, **323**, 795.

Emslie, A.G. 1980, *Ap. J.*, **235**, 1055.

Evans R.D. 1955, it The Atomic Nucleus, McGraw-Hill, New York.

Ho, C. 1986, *M.N.R.A.S.*, **221**, 523.

Jackson, J.D. 1962, *Classical Electrodynamics*, Wiley, New York, Chapter 12.

Kundu, M.R. 1983, *Solar Phys.*, **86**, 205.

Leach, J. and Petrosian, V. 1981, *Ap. J.*, **251**, 781.

Leach, J. and Petrosian, V. 1983, *Ap. J.*, **269**, 715.

Leach, J. 1984, Ph.d. Thesis, Stanford University.

Leach, J. , Emslie, A.G. and Petrosian, V. 1985, *Solar Phys.*, **96**, 331.

Lu, E.T. and Petrosian, V. 1989, *Ap. J.*, **338**, 1122.

MacKinnon, A.L. and Brown, J.C., 1988, Preprint.

Matz, S.M., Forrest, D.J., Vestrand, W.T., Chupp, E.L., Share, G.H., Rieger, E. 1985, *Ap. J. (Letters)*, **288**, L37.

Petrosian, V. 1985, *Ap. J.*, **299**,987.

Ramaty, R., Murphy, R.J., Kozlovsky, B. and Lingenfelter, R.E. 1983, *Solar Phys.*, **86**, 395.

Snyder, H.S. and Scott W.T. 1949, *Phys. Rev.*, **76**, 220.

Table 1

A comparison of analytic widths with numerical results for 10.6 MeV electrons, with $\delta = 5$, $\alpha_o^2 = 0.04$, 0.10, 0.40, and 40, at depth $\tau_c = \eta$. The subscript $*$ denotes a numerical result.

$4/E\alpha_o^2$	$\delta\alpha_o^2/2$	α_o^2	$\alpha_c^2(\eta)$	$\tilde{\alpha}_c^2(\eta)$	$\alpha_*^2(\eta)$
5.00	0.10	0.04	0.13	0.12	0.11
2.00	0.25	0.10	0.20	0.16	0.17
0.50	1.00	0.40	0.50	0.31	0.31
0.005	100.0	40.0	40.10	0.81	0.61

Table 2

Critical values for the dispersion α_D^2 and depth τ_{sd}.

E	16 keV	300 keV	1 MeV	10.6 MeV
α_D^2	0.09	0.01	3.50×10^{-3}	1.80×10^{-4}
τ_{sd}	0.83	3.40	7.00	42.0

Table 3

Spectral indices of the spatially integrated flux F_r for energy ranges 16 to 300 keV, 600 keV to 5.32 MeV and 10.6 to 76 MeV, respectively.

	$R_o = 3 \times 10^{-3}$			$R_o = 1.3$		
α	m_x	m_m	m_γ	m_x	m_m	m_γ
Beam, $\alpha_o^2 = 0.40$						
54°	4.00	4.20	5.62	4.16	5.68	5.99
126°	4.23	6.86	14.7	5.17	14.3	15.9
Pancake, $\alpha_o^2 = 0.40$						
54°	3.98	3.99	5.55	4.14	5.46	5.99
126°	4.15	6.41	20.3	4.88	17.4	19.6
Isotropic, $\alpha_o^2 = \infty$						
54°	3.98	4.03	5.57	4.13	5.50	5.99
126°	4.18	5.87	24.7	5.00	17.6	19.6
Isotropic, $\alpha_o^2 = \infty$, *convergent*						
54°	3.98	3.99	5.06	4.03	5.18	6.00
126°	4.17	5.72	11.2	4.39	15.5	14.6

Table 4

Spectral indices of $F_{\rm TOT}$ for $\delta = 5$ and $\alpha_o^2 = 0.40$.

	Beam			*Pancake*		
R_o	m_x	m_m	m_γ	m_x	m_m	m_γ
0	3.20	3.91	4.05	3.22	3.90	4.05
3×10^{-3}	3.20	3.94	4.92	3.22	3.97	5.54
1.3	3.32	4.86	5.80	3.40	5.38	5.97
3×10^{3}	3.50	6.11	6.02	4.38	5.83	5.98

Table 5

Spectral indices of F_τ for different pitch angles for various flare models. The quantities m_x and m_γ vare as defined for Table 3.

				$\alpha = 54°$		$\alpha = 126°$	
α_o^2	α_1	B_o(G)	b	m_x	m_γ	m_x	m_γ
0.40	0	100	1	4.05	4.06	4.89	10.30
0.40	$\pi/2$	100	1	3.96	4.02	4.54	9.89
0.40	0	2000	1	4.04	4.20	4.89	12.70
0.40	$\pi/2$	2000	1	3.96	4.18	4.54	12.8
0.40	0	10^4	1	4.03	9.62	4.83	24.00
0.40	$\pi/2$	10^4	1	3.98	10.0	4.53	26.30
∞	–	100	1	3.98	4.02	4.65	9.93
∞	–	100	2	3.94	4.05	4.39	5.02
∞	–	100	5	4.04	4.06	4.43	5.00
∞	–	100	10	4.18	4.10	4.47	4.98
0.04	0	100	2	4.13	4.05	5.27	4.99
∞	–	2000	1	3.98	4.17	4.65	13.10
∞	–	2000	10	4.35	7.94	4.60	6.12

Table 6

Spectral indices of $F_{\rm TOT}$ for the flare models of Table 5. $\Delta m = m_\gamma - m_x$.

α_o^2	α_1	B_o(G)	$B_{\rm tr}/B_o$	m_x	m_m	m_γ	Δm
0.40(b)	0	100	1	3.21	3.91	4.03	0.83
0.40(p)	$\pi/2$	100	1	3.22	3.91	4.04	0.82
0.40(b)	0	2000	1	3.21	3.91	4.07	0.86
0.40(p)	$\pi/2$	2000	1	3.23	3.93	4.32	1.09
0.40(b)	0	10^4	1	3.19	3.96	4.65	1.46
0.40(p)	$\pi/2$	10^4	1	3.28	4.27	6.00	2.72
∞	–	100	1	3.21	3.91	4.03	0.83
∞	–	100	2	3.22	3.89	4.03	0.81
∞	–	100	5	3.38	3.91	4.06	0.68
∞	–	100	10	3.52	3.95	4.11	0.59
0.04(b)	0	100	2	3.19	3.19	4.03	0.84
∞	–	2000	1	3.21	3.91	4.16	0.95
∞	–	2000	10	3.67	4.44	5.01	1.33

Figures

Figure 1.– Electron flux (arbitrary units) vs. pitch angle (degrees) for the collision-only case with $E = 10.6$ MeV, $\delta = 5$, $\alpha_1 = 0$, $\alpha_o^2 = 0.40$, $n_e = \text{const.} = 10^{10}\text{cm}^{-3}$, and constant B. The analytic results, from equation (15), are given by o's and the numerical results by solid lines. Each curve is labeled by the value of τ_c/η.

Figure 2.– Electron Flux vs. pitch angle at $\tau_c = \eta$, for 16 keV, 1 MeV and 10.6 MeV electrons for the collision dominated ($R_o = 3 \times 10^{-9}$) model with $\delta = 5$, $\alpha_1 = 0$ and $\alpha_o^2 = 0.40$. Each curve is labeled by the value of the electron energy in MeV. The solid lines are the numerical results, and the o's are the analytic results. The flux has been normalized to 1.0 at $\alpha = 0$.

Figure 3.– Same as Figure 2, for the pancake injection model ($\alpha_1 = \pi/2$) with $\delta = 5$, and $\alpha_o^2 = 0.40$. There are no analytic results for this case.

Figure 4.– The Flux integrated over depth F_τ versus pitch angle for the beam ($\alpha_1 = 0$, solid lines) and pancake ($\alpha_1 = \pi/2$, dashed lines) models with $R_o = 3 \times 10^{-9}$, $\delta = 5$ and $\alpha_o^2 = 0.40$, for 300 keV and 10.6 MeV.

Figure 5.– The flux integrated over pitch angle F_μ versus normalized column depth τ_c/η for the model with $\alpha_1 = 0$, $\alpha_o^2 = 0.40$ and $R_o = 3 \times 10^{-9}$. The lines reperesent numerical results and the o's the analytic results from equation (17). These curves, labeled by the value of the electron energy in MeV, are nearly independent of the injection parameters such as δ, α_o^2, etc ...

Figure 6.– Electron flux versus pitch angle for the synchrotron dominated case with $R_o = 3 \times 10^3$, at $\tau_s = 1$ for $\alpha_1 = 0$, $\alpha_o^2 = 0.40$, with each curve labeled by the value of the electron energy in MeV. Solid lines represent numerical results, and the o's the analytic results from equation ($A.24$). The dashed line depicts the injected flux. All the fluxes are normalized to the flux at $\tau_s = 0$, $\alpha = 0$.

Figure 7.– Flux at zero pitch angle versus energy, for the model with $R_o = 3 \times 10^3$. The dashed lines are the analytic results of equation (A.24), and the solid lines are the numerical results; all are labeled with the appropriate value of τ_s. Here the flux is multiplied by E^δ, so that the curve for zero depth is flat.

Figure 8.– The Flux integrated over depth F_τ versus pitch angle for the beam (solid lines) and pancake (dashed lines) models with $R_o = 1.3$, $\delta = 5$ and $\alpha_o^2 = 0.40$, and 300 keV and 10.6 MeV electrons.

Figure 9.– Flux integrated over pitch angle F_μ multiplied by E^δ versus electron energy for the models with $\delta = 5$, $\alpha_o^2 = 0.40$, and $R = 1.3$. The curves are labeled with the appropriate values of τ_s. The solid lines are for $\alpha_1 = 0$ (beam) and the dashed lines are for $\alpha_1 = \pi/2$ (pancake).

Figure 10.– Electron flux versus pitch angle at the top of the loop ($s = 0$) for the 'short' converging field cases with $\delta = 5$, $\alpha_o^2 = \infty$ and $b = 10$. The solid lines are for the case with $R_o(\text{top}) = 3 \times 10^{-3}$ at the top, the dashed lines are for $R_o(\text{top}) = 1.3$ and each curve is labeled by the value of the electron energy in MeV. The 16 keV results have been shifted by 10^{-10}, and the 1 MeV results have been shifted by 10^{-3}.

Figure 11.– Normailized electron flux versus pitch angle for 10.6 MeV at $\tau_c = \eta$, $\delta = 5$ and $\alpha_o^2 = \infty$. Curves labeled "U" are for the uniform field cases and curves labeled "C" are for the 'long' convergence cases with $S_b = 3.7 \times 10^{-9}\text{cm}^{-1}$. The solid lines are for the models with $R_o = 3 \times 10^{-9}$ at the top, and dashed lines are for cases with $R_o = 1.3$ at the top.

Figure 12.– Normailzed electron flux versus pitch angle for the flare model with $\delta = 3.75$, $\alpha_o^2 = \infty$, and $b = 10$. The solid lines are for $\tau_c = 0$, and the dashed lines are for $\tau_c = \eta$. Each curve is labeled by the value of the electron energy in MeV.

Figure 13.– Electron flux versus pitch angle for 1 MeV electrons for a model with a density of Fe ions of $10^{27}\mathrm{cm}^{-3}$ and a magnetic field of 10^{12} G (or $R_o = 1.2$). The curves are labeled by the value of $\tau_c \approx \tau_s$.

Figure 1

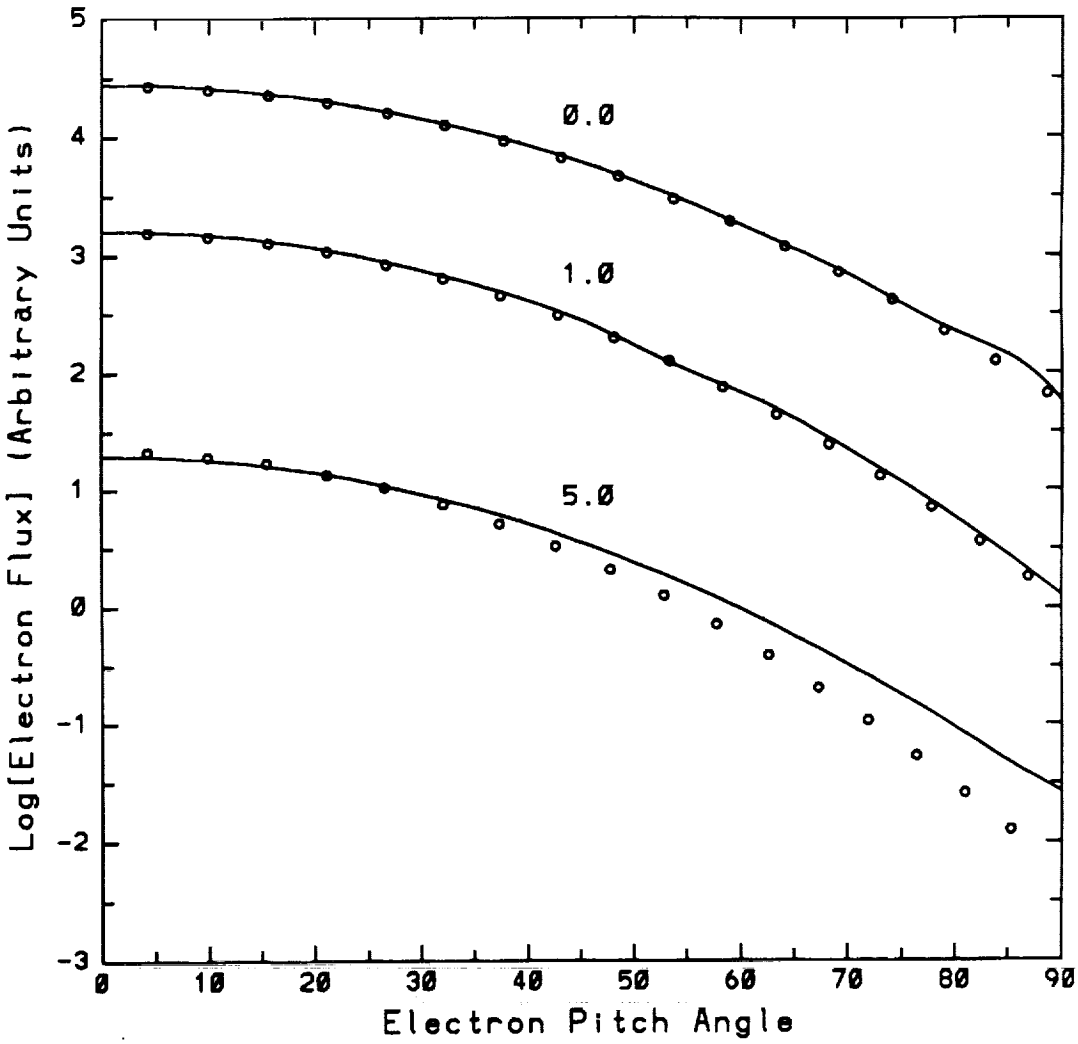
Log[Electron Flux] (Arbitrary Units)
5
4
3
2
1
0
-1
-2
-3
0.0
1.0
5.0
0
10
20
30
40
50
60
70
80
90
Electron Pitch Angle

Figure 2

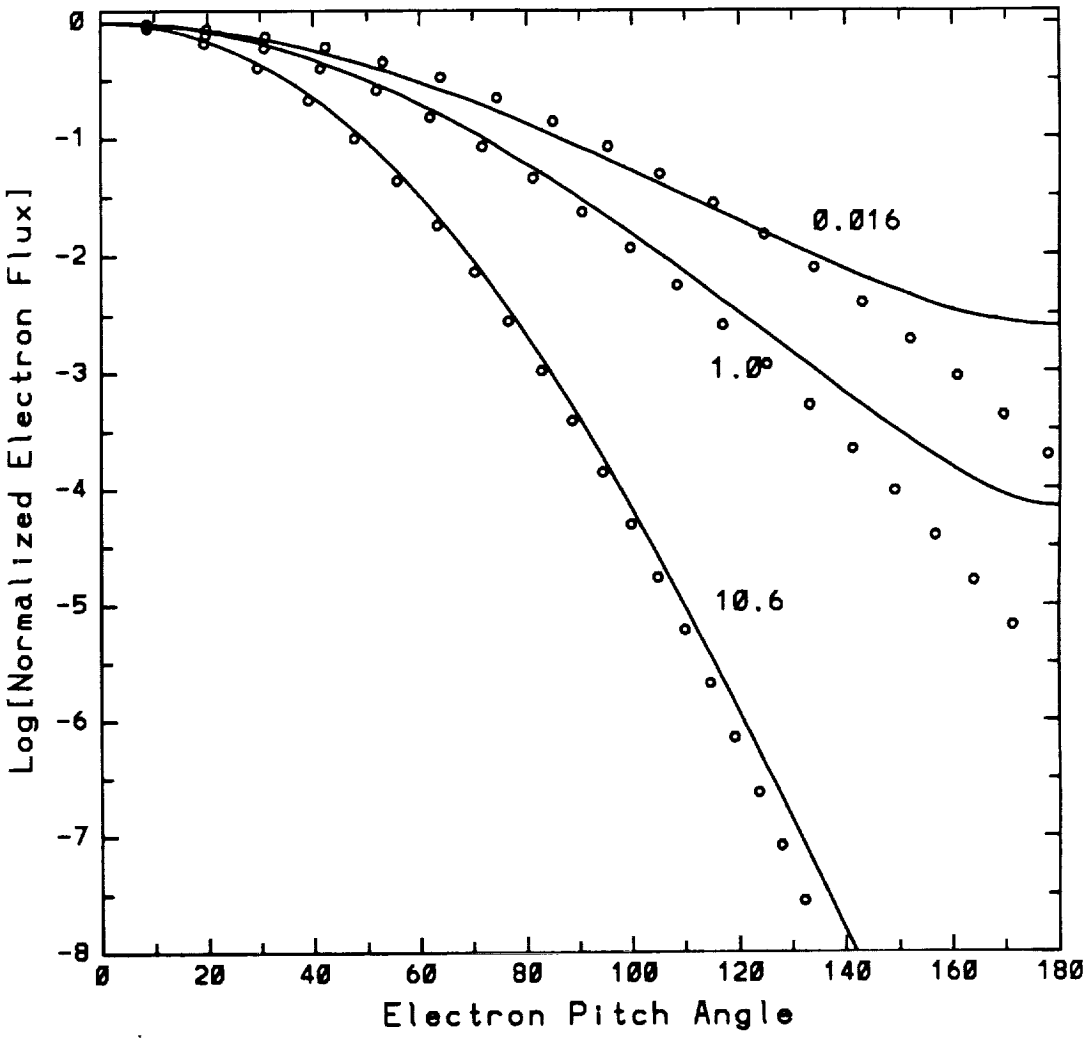
Log[Normalized Electron Flux]
0
-1
-2
-3
-4
-5
-6
-7
-8
0
20
40
60
80
100
120
140
160
180
Electron Pitch Angle
0.016
1.0
10.6

Figure 3

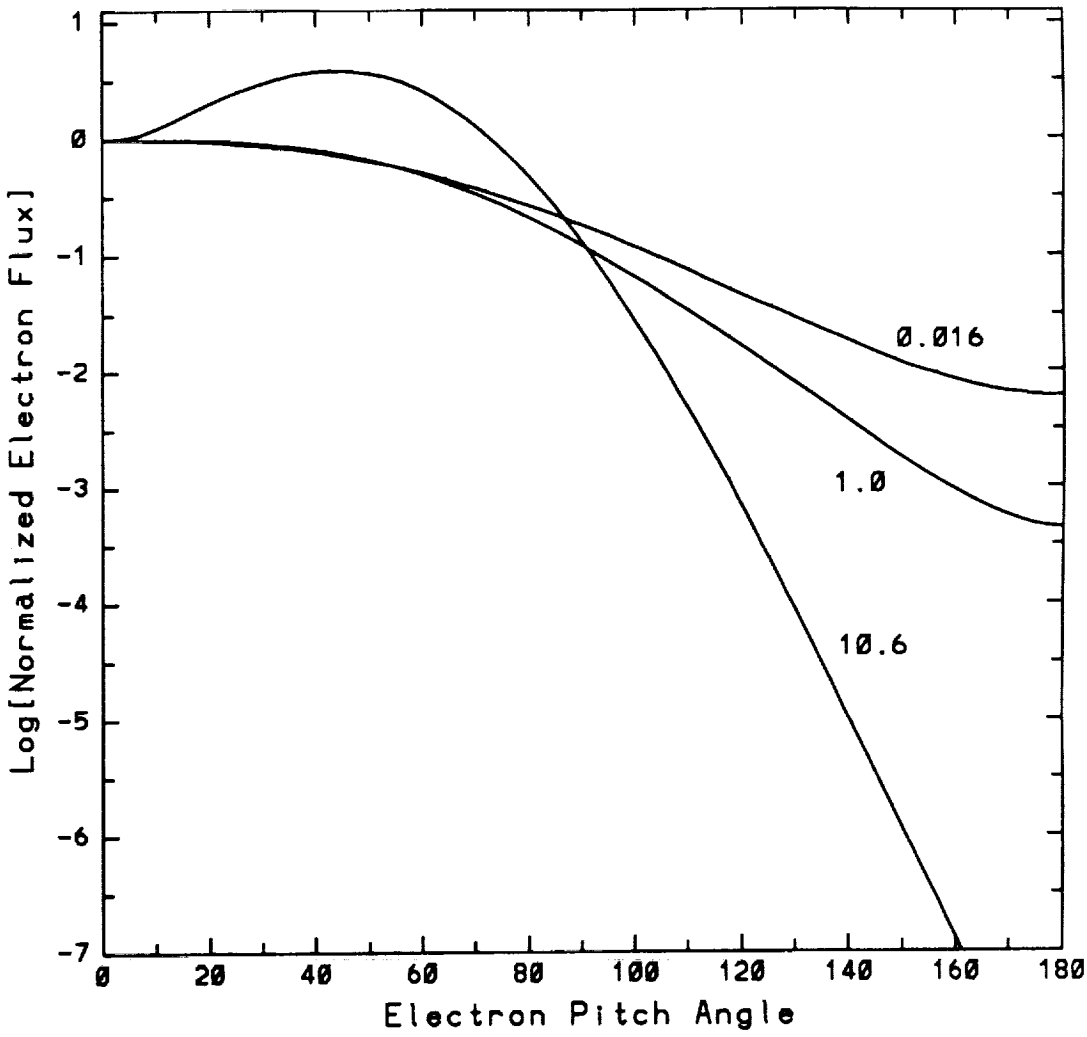
1
0
-1
-2
-3
-4
-5
-6
-7
Log[Normalized Electron Flux]
0
20
40
60
80
100
120
140
160
180
Electron Pitch Angle
0.016
1.0
10.6

Figure 4

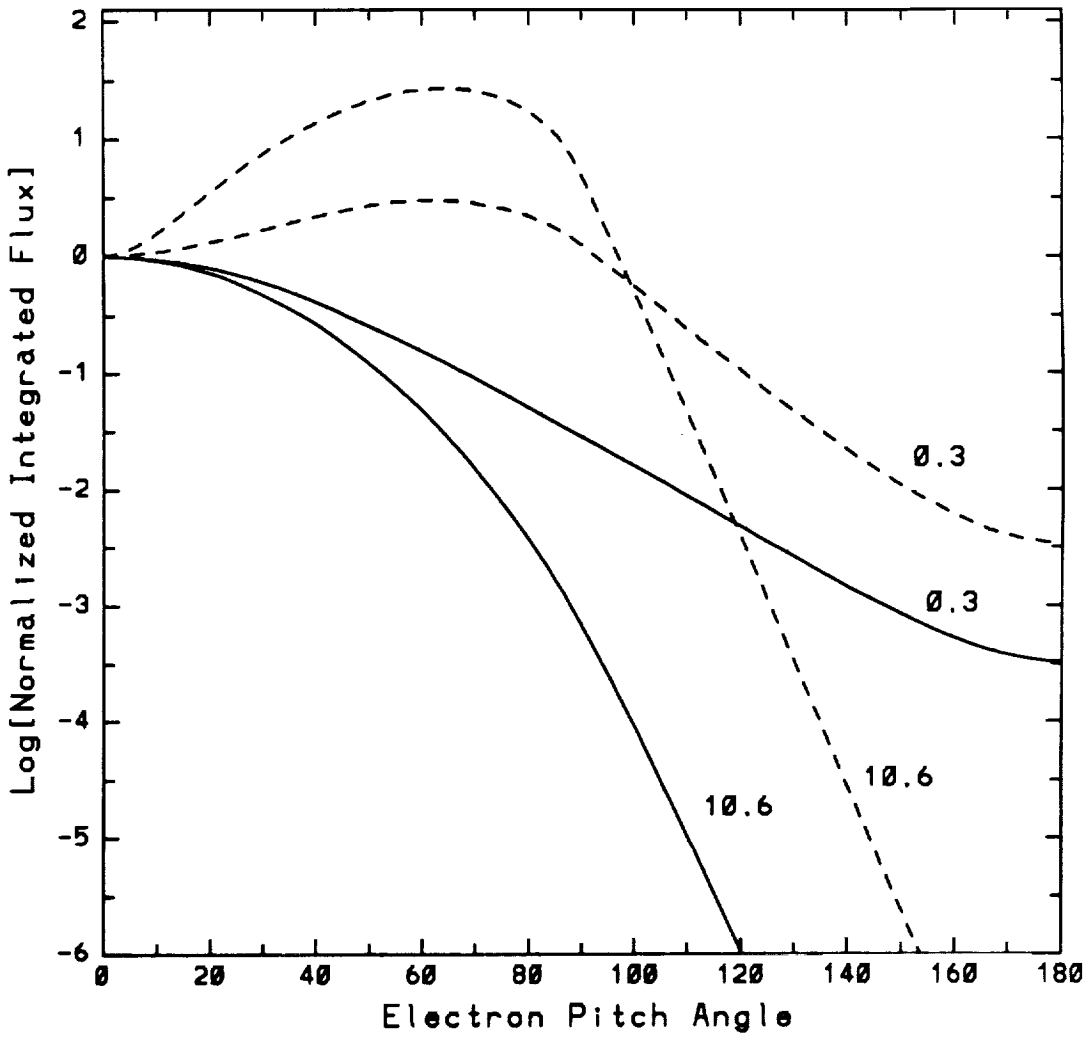
Log[Normalized Integrated Flux]
Electron Pitch Angle
2
1
0
-1
-2
-3
-4
-5
-6
0
20
40
60
80
100
120
140
160
180
0.3
0.3
10.6
10.6

Figure 5

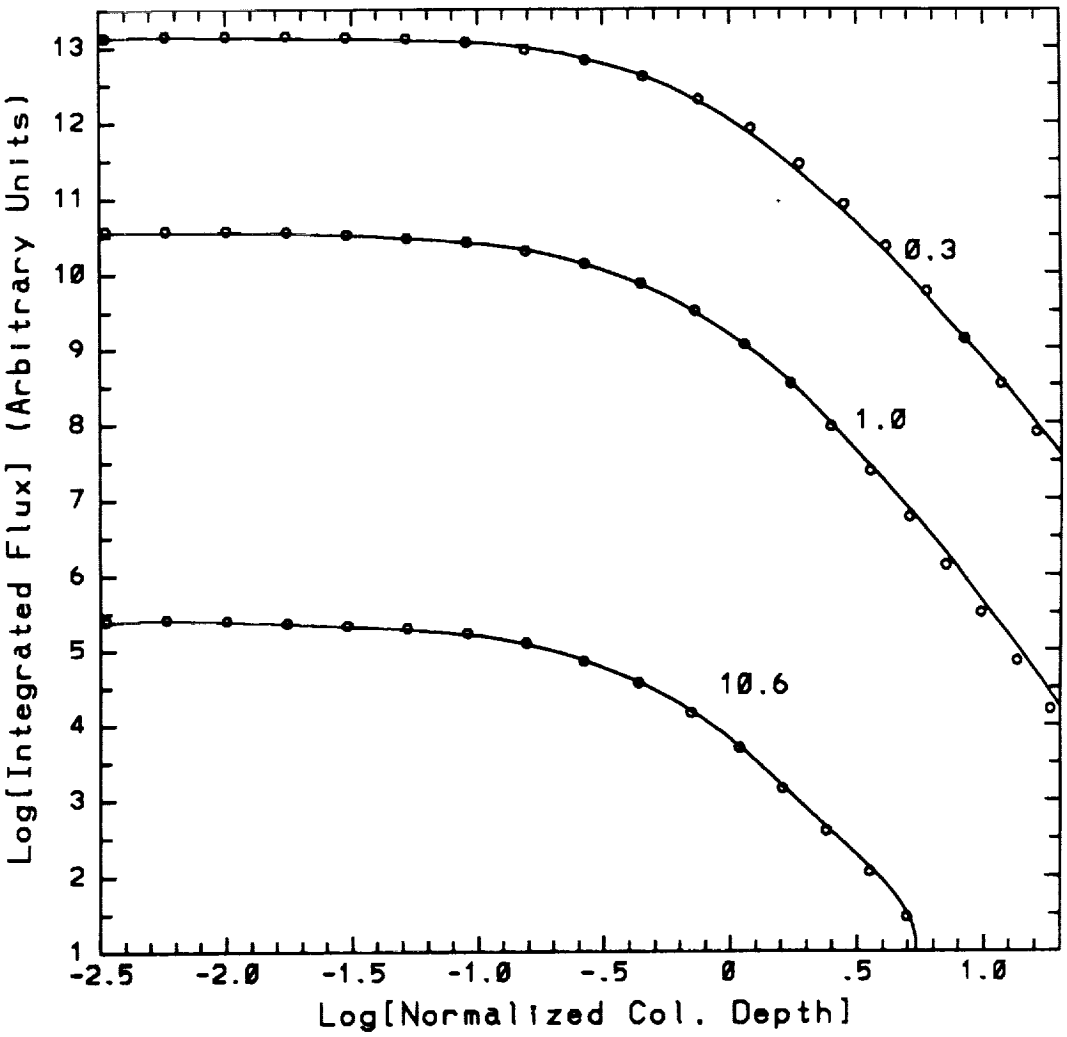
Log[Integrated Flux] (Arbitrary Units)
13
12
11
10
9
8
7
6
5
4
3
2
1
-2.5
-2.0
-1.5
-1.0
-.5
0
.5
1.0
Log[Normalized Col. Depth]
0.3
1.0
10.6

Figure 6

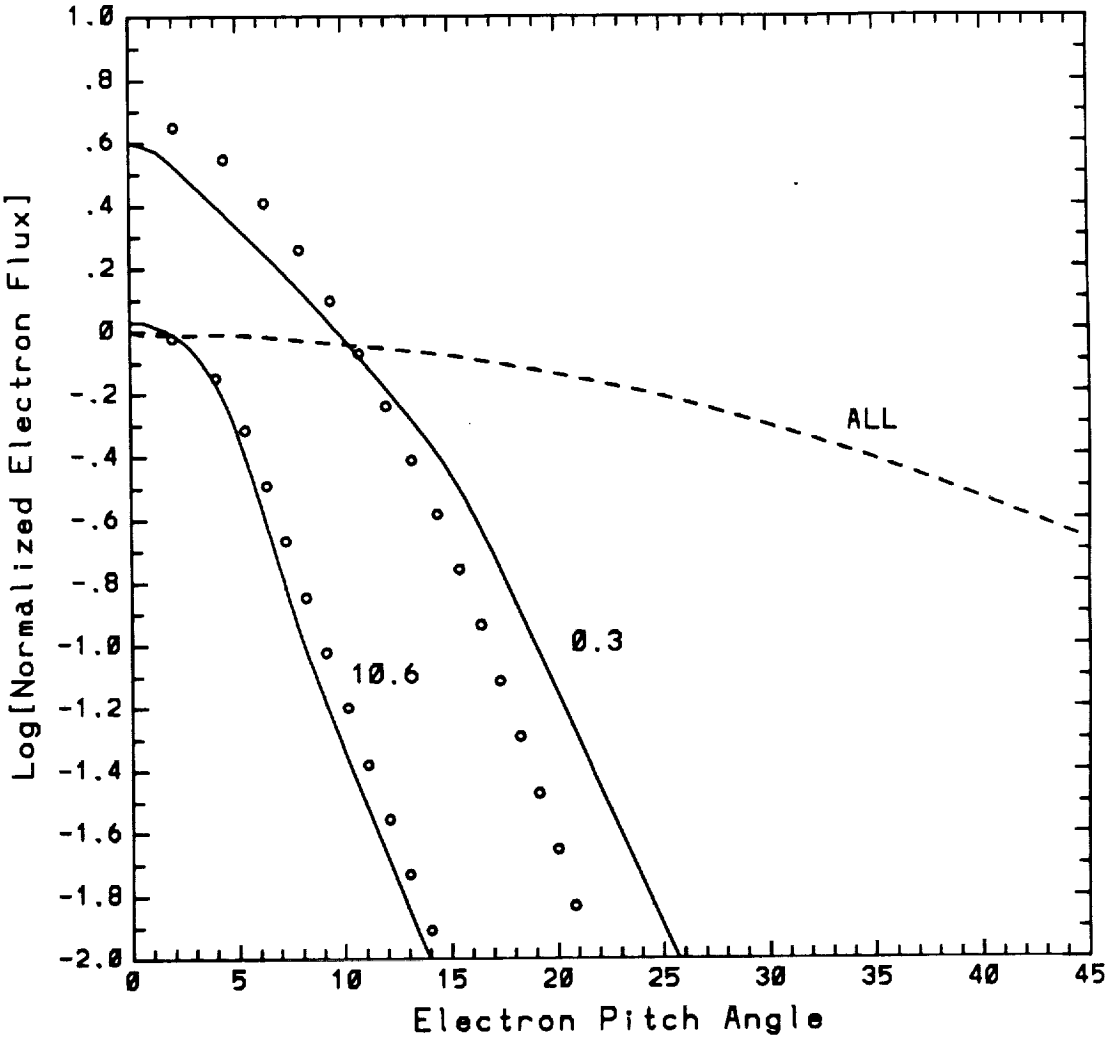
1.0
.8
.6
.4
.2
0
-.2
-.4
-.6
-.8
-1.0
-1.2
-1.4
-1.6
-1.8
-2.0
Log[Normalized Electron Flux]
0
5
10
15
20
25
30
35
40
45
Electron Pitch Angle
ALL
0.3
10.6

Figure 7

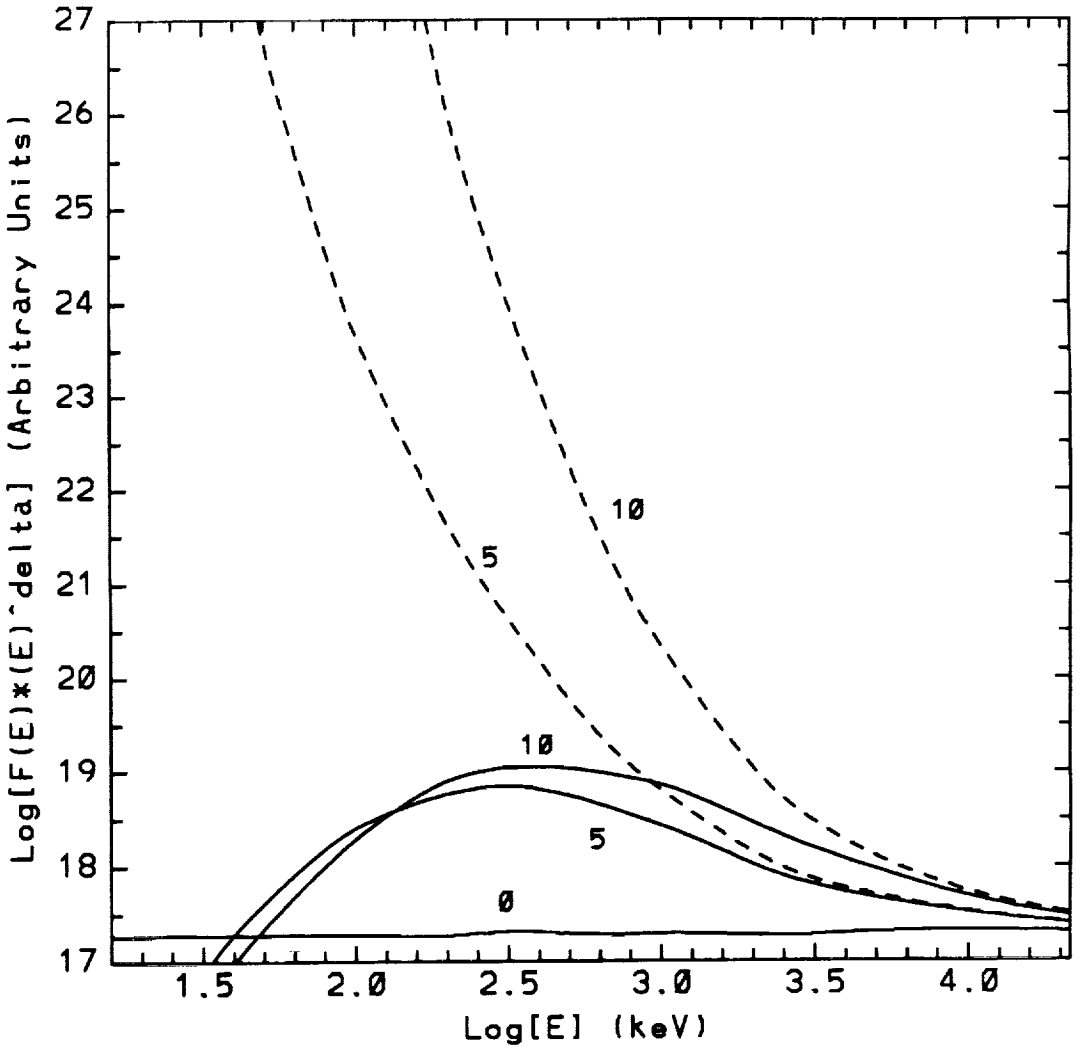
Log[F(E)*(E)^delta] (Arbitrary Units)
27
26
25
24
23
22
21
20
19
18
17
1.5
2.0
2.5
3.0
3.5
4.0
Log[E] (keV)
10
5
10
5
0

Figure 8

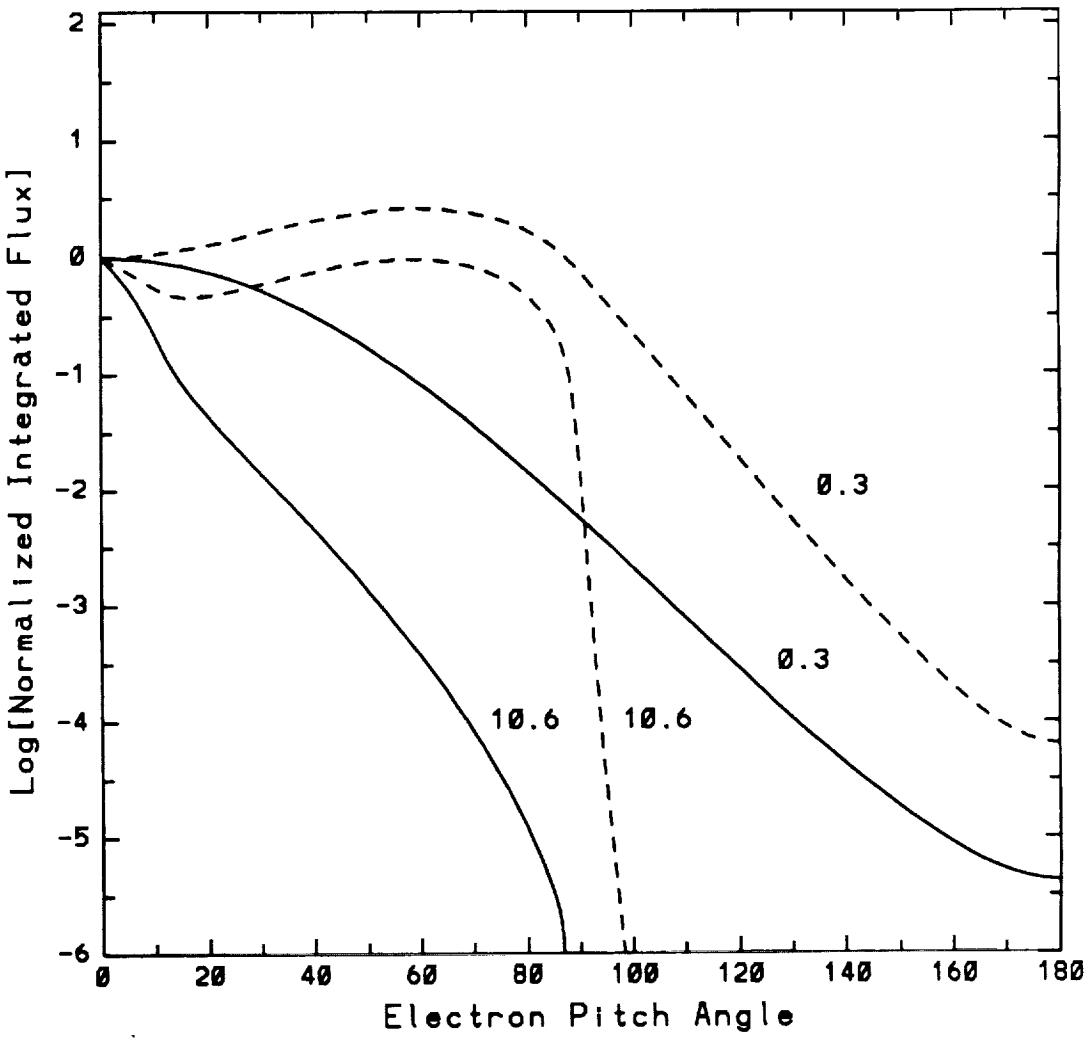
2
1
0
-1
-2
-3
-4
-5
-6
Log[Normalized Integrated Flux]
0
20
40
60
80
100
120
140
160
180
Electron Pitch Angle
0.3
0.3
10.6
10.6

Figure 9

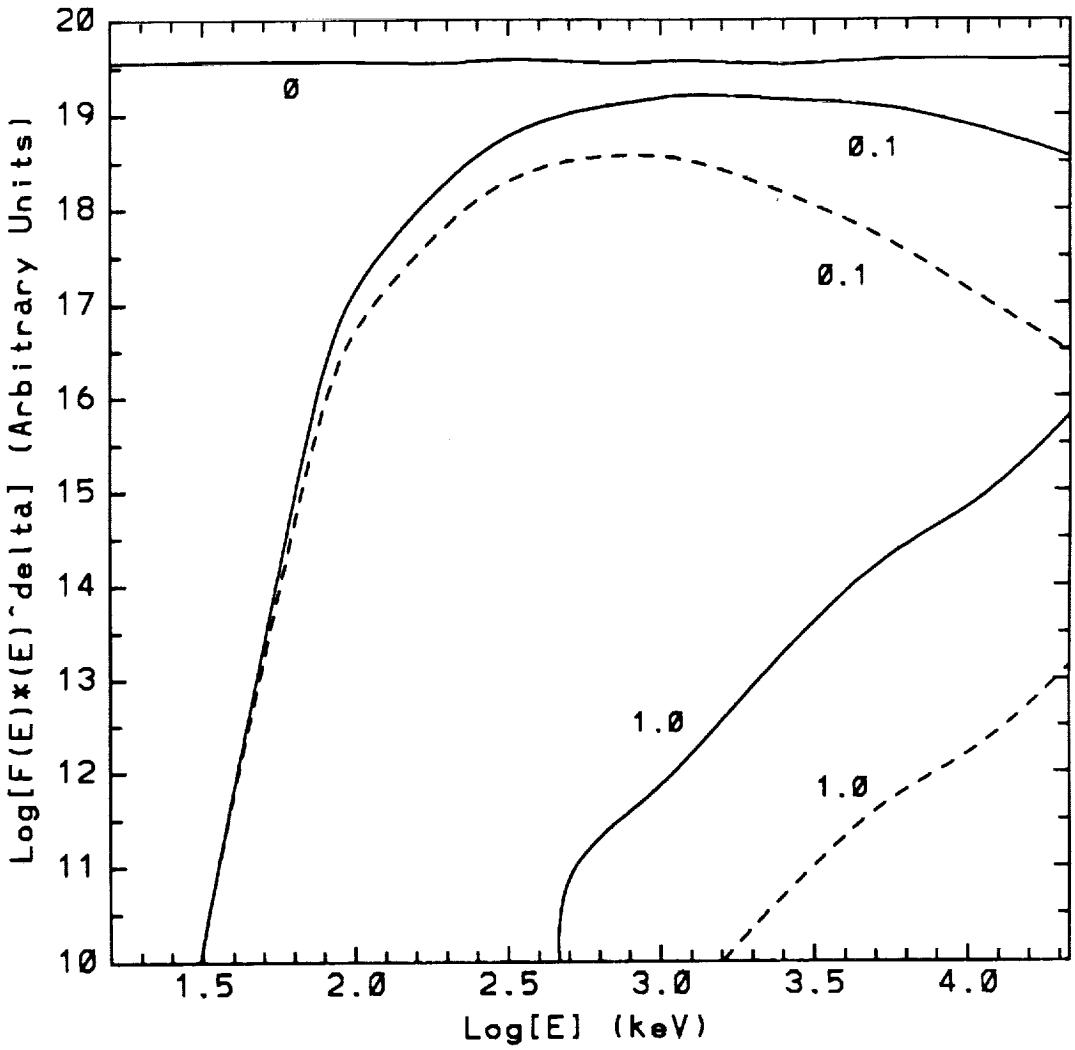
20
19
18
17
16
15
14
13
12
11
10
Log[F(E)*(E)^delta] (Arbitrary Units)
1.5
2.0
2.5
3.0
3.5
4.0
Log[E] (keV)
0
0.1
0.1
1.0
1.0

Figure 10

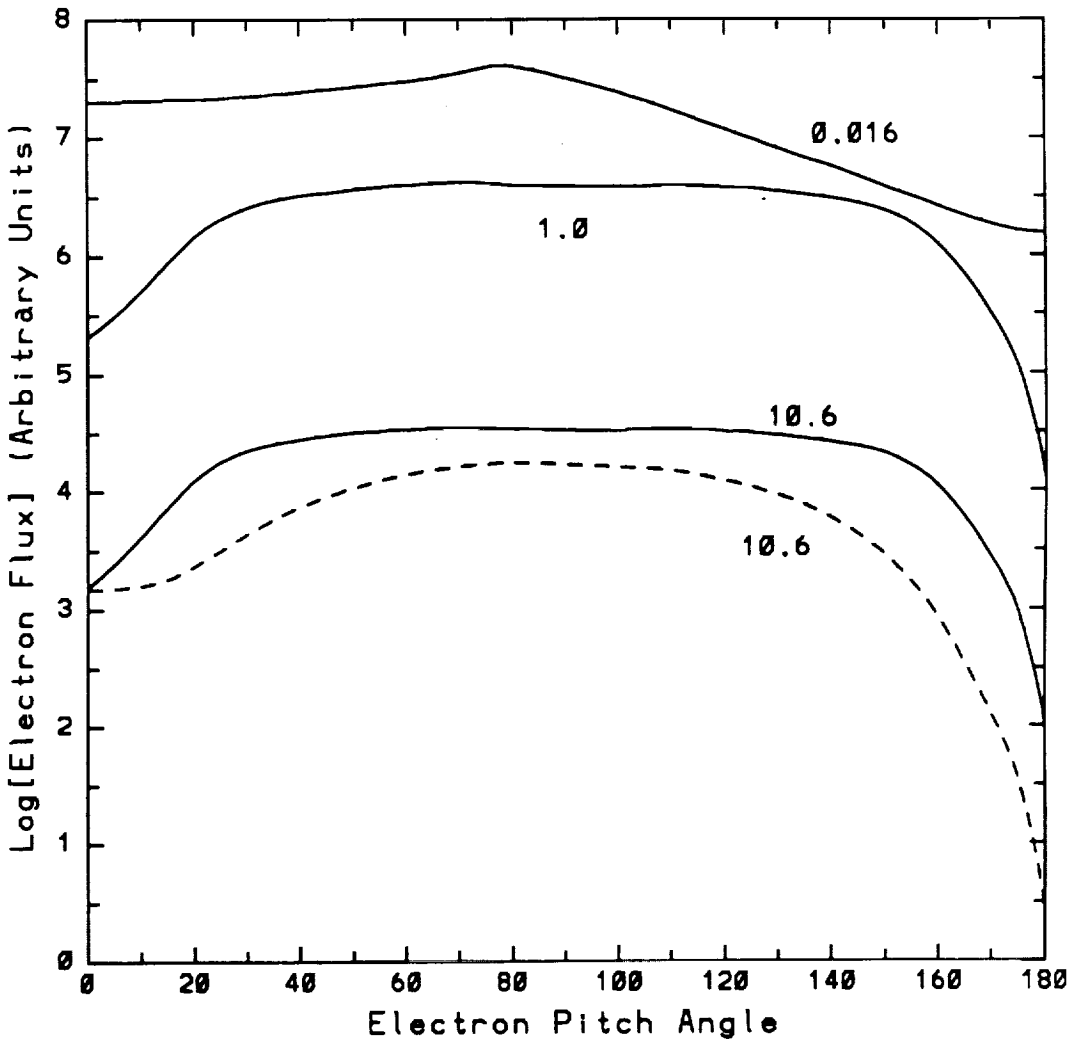
Log[Electron Flux] (Arbitrary Units)
Electron Pitch Angle
0.016
1.0
10.6
10.6
0
1
2
3
4
5
6
7
8
0
20
40
60
80
100
120
140
160
180

Figure 11

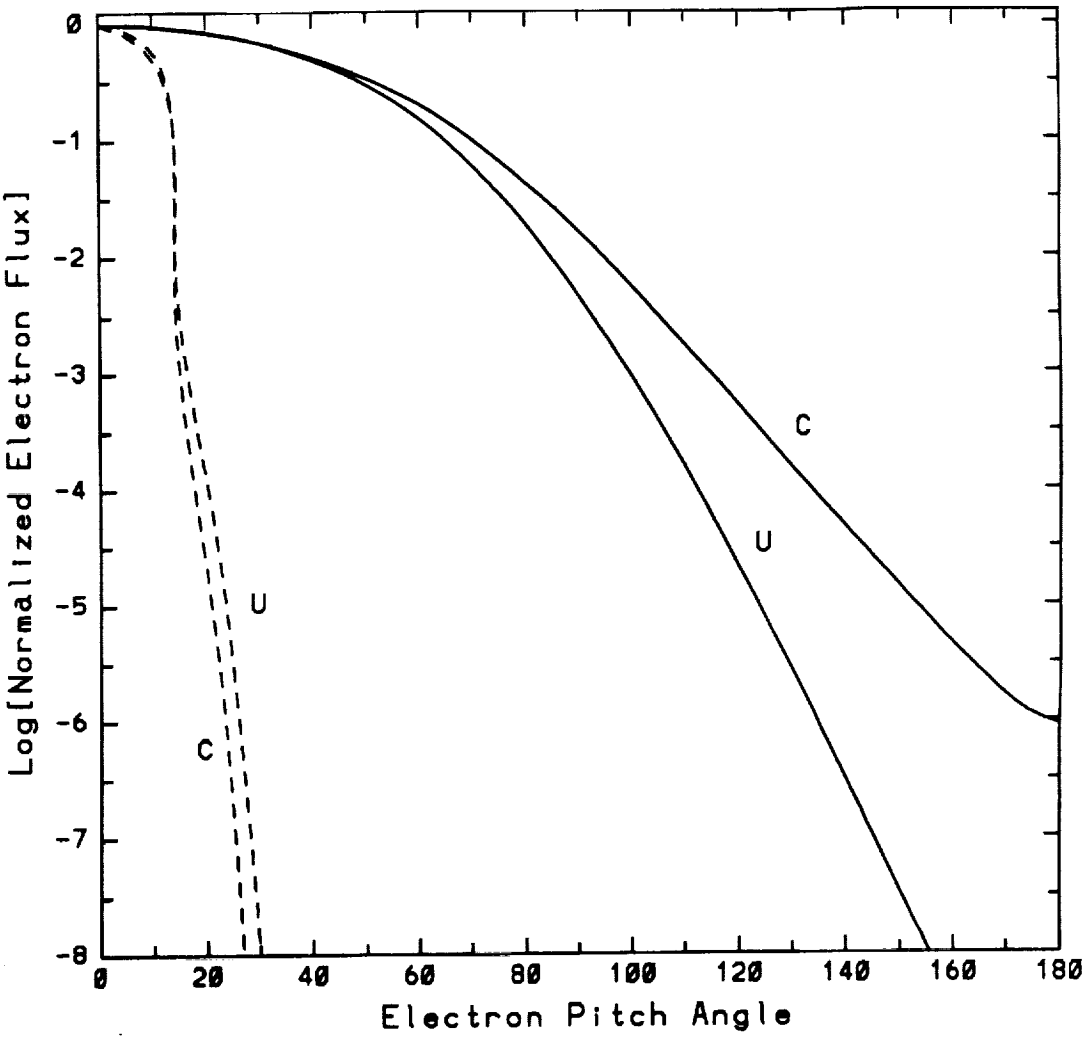
Log[Normalized Electron Flux]
0
-1
-2
-3
-4
-5
-6
-7
-8
0
20
40
60
80
100
120
140
160
180
Electron Pitch Angle
C
U
U
C

Figure 12

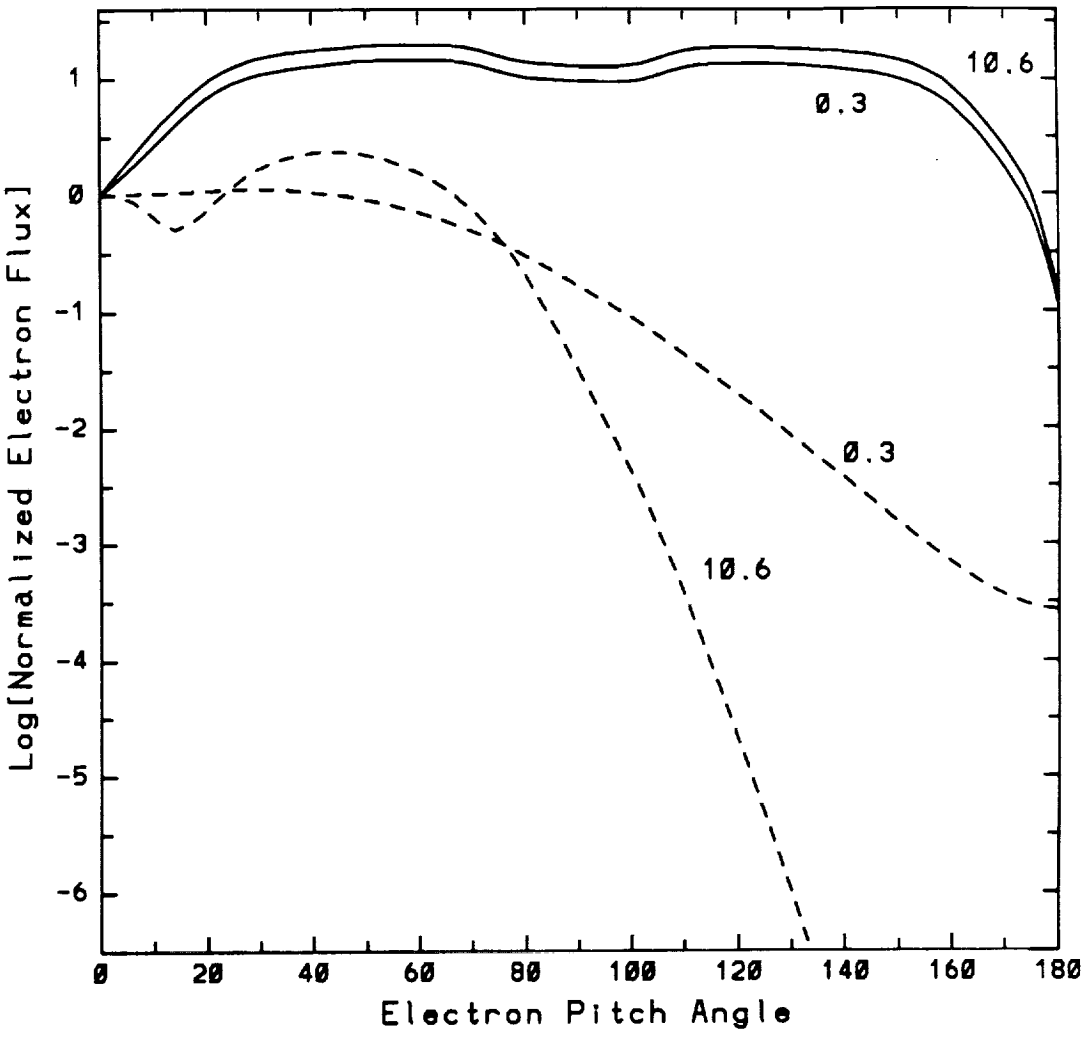
10.6
0.3
0.3
10.6
1
0
-1
-2
-3
-4
-5
-6
0
20
40
60
80
100
120
140
160
180
Log[Normalized Electron Flux]
Electron Pitch Angle

Figure 13

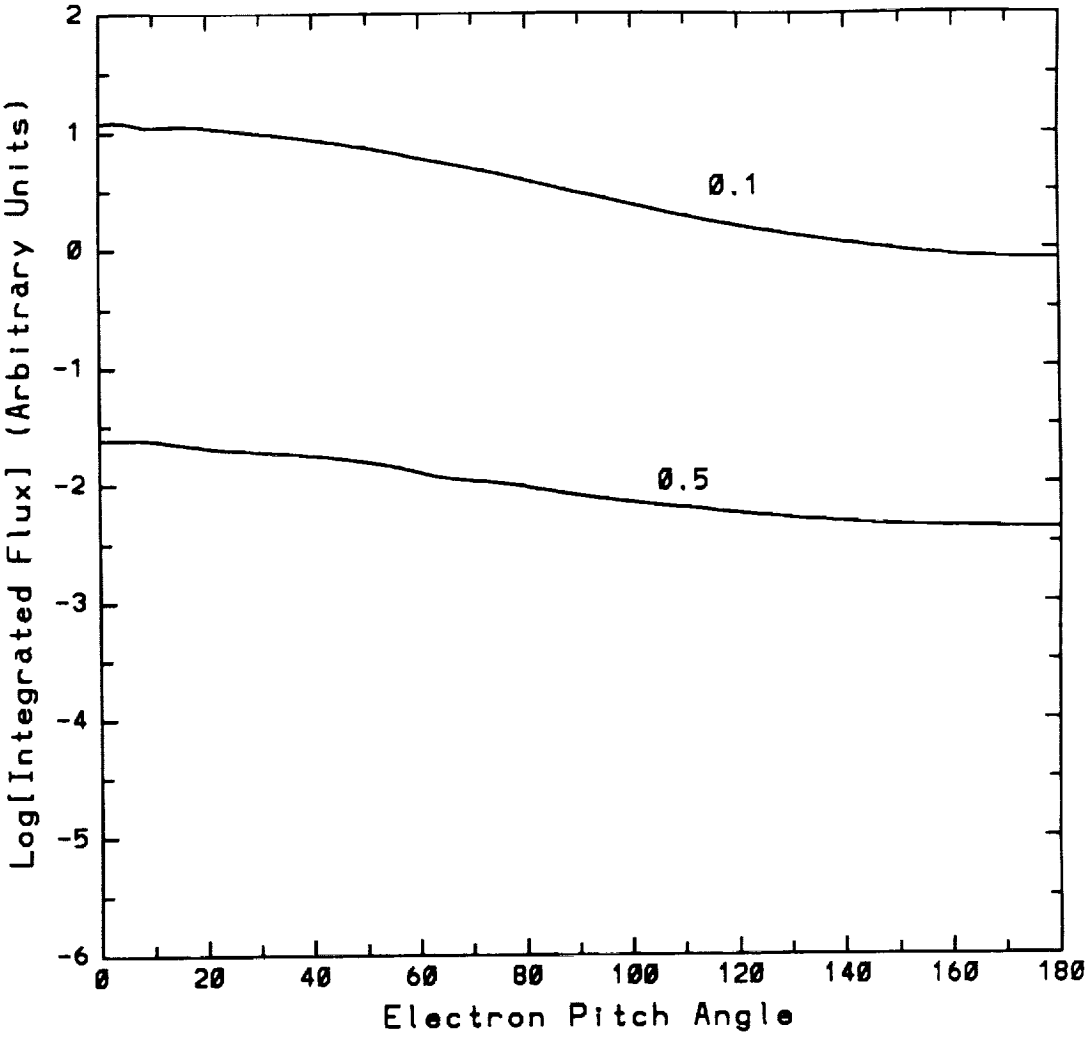
2
1
0
-1
-2
-3
-4
-5
-6
Log[Integrated Flux] (Arbitrary Units)
0.1
0.5
0
20
40
60
80
100
120
140
160
180
Electron Pitch Angle

Addresses

James M.McTiernan: Space Sciences Laboratory, University of California, Berkeley, CA 94720

Vahé Petrosian: Center for Space Science and Astrophysics, Stanford, CA 94305